Development of Bacteria-Based Bio-Hybrid Delivery Systems: Fabrication, and Characterization of Chemotaxis and Quorum Sensing

Ali Akbar Sahari

Dissertation submitted to the faculty of the Virginia Polytechnic Institute and State University in partial fulfillment of the requirements for the degree of

Doctor of Philosophy
in
Biomedical Engineering

Chair: Bahareh Behkam

Lissett R. Bickford

Rafael V. Davalos

Birgit E. Scharf

Ann M. Stevens

September 2, 2014
Blacksburg, VA

Keywords: bio-hybrid systems, microfluidics, drug delivery, chemotaxis, quorum sensing

Development of Bacteria-Based Bio-Hybrid Delivery Systems: Fabrication, and Characterization of Chemotaxis and Quorum Sensing

Ali Akbar Sahari

Abstract

Bio-hybrid approaches have recently provided a possible solution to address the challenge of on-board actuation, control and communication modules for micro/nanoscale cargo-carrying vehicles by integrating live prokaryotic or eukaryotic cells with synthetic objects. More specifically, because micro/nanoparticles are able to transport cargos efficiently and bacteria can play the role of targeted and selective delivery agents, a hybrid of these two can advance the current strategies for environmental monitoring, drug delivery and medical imaging. The main goal of this dissertation was to fabricate, assemble, and characterize different components of a mobile network of bacteria-based bio-hybrid systems for long-term applications in drug delivery and biosensing. First, a new library of bacteria-enabled delivery systems was developed by coupling live engineered bacteria with non-spherical particles and the transport of these bacteria-based systems was investigated in the absence and presence of chemical cues using microfluidic platforms. Next, a quorum-sensing (QS) based bacterial cell-cell communication network was characterized in a high-throughput manner in order to understand the coordinated behavior of the bacterial species ferrying the cargoes. Lastly, the QS behavior of a chemotactic population of the bacterial species in response to the endogenously produced signaling molecules was studied. The work presented in this dissertation lays the foundation for a well-characterized generation of bacteria-assisted cargo delivery devices with enhanced transport properties and capable of executing pre-programmed multi-agent coordinated tasks upon their arrival at the target site.

Dedication

I dedicate this dissertation to my parents, Sherafat and Esmaeil. I hope this achievement has completed the dream that you had for me many years ago.

Acknowledgements

I would like to sincerely thank my advisor and mentor, Dr. Bahareh Behkam, for giving me the opportunity to work in her lab, and the constant and relentless support of my Ph.D. work with her insightful advice, patience, understanding and enthusiasm. The conversations we have had, both work-related and unrelated, have been stimulating, challenging and most importantly, enjoyable. I am also very grateful to my committee members; Dr. Birgit E. Scharf deserves special recognition, her advice, encouragement, training and relentless support have greatly helped me during my intellectual journey as a graduate student. Dr. Rafael Davalos, Dr. Ann Stevens and Dr. Lissett Bickford deserve many thanks for their helpful discussions, support and encouragement along the way.

On a more personal note, I would like to thank my very special friends, Dr. Omidreza Shoghli, Dr. Behnam Bahrak, Arash Jahangiri, Sahar Ghanipoor, Yahya Hosseini and Dr. Nima Toosizadeh, whom have helped me along the way and I consider more than friends. I am grateful for their friendship and moral support throughout all the years in graduate school and away from home. I also would like to thank my past and present colleagues at the MicroN BASE laboratory, especially Aziz Traore, Brian Geuther, Chris Suh, Ahram Kim, Zhou Ye, Devon Headen, and Meghan Canter for making the day to day life in the lab something to look forward to and for offering support and intellectual input during the past five years. Special thanks also go to all members of Dr. Biswarup Mukhopadhyay's lab, especially Jason Rodriguez, for their help. I am also very grateful to Revathy Ramachandran from Dr. Ann Stevens' lab, for her helpful discussions and experimental protocols. Virginia Tech was a wonderful place for me to complete my graduate studies. I have immensely profited from this rich and safe environment to conduct my Ph.D. research. I would like to specifically acknowledge the facilities provided by the Micro and Nanofabrication laboratory at

Virginia Tech, Virginia Bioinformatics Institute and the funding sources provided by the Department of Mechanical Engineering and the National Science Foundation, without which, this research would not have been possible.

Table of Contents

List of Figures

List of Tables

Chapter 1: Introduction

1.1 Motivation and problem statement

Mobile microrobots can travel to previously inaccessible small spaces and are envisioned to impact the field of microrobotics as inexpensive agents of distributed networks of swarm robotic systems. The potential applications of such microrobots include biosensing and environmental monitoring, minimally invasive diagnosis, targeted drug delivery and localized treatment of diseases [1]. With the recent advances in micro/nanofabrication and assembly methods, truly microscale robotic systems with characteristic dimensions less than 100 μm have been realized [2, 3]. However, these microrobots were actuated and controlled by off-board magnetic fields. Realization of on-board actuation along with communication and control modules are among the most significant challenges towards realization of microscale mobile robots with advanced functionalities. Over the past few years, bio-hybrid approaches have been widely employed as a possible solution to address these challenges by integrating live prokaryotic or eukaryotic cells within robotic systems [4-10]. The most widely used of such living cells that can be exploited as on-board actuators are flagellated bacteria with the purpose of using bacteria for actuation, sensing, communication, and control. Since micro/nanoparticles are able to transport cargos efficiently and bacteria can play the role of targeted and selective delivery agents, a hybrid of these two can specifically advance the current strategies for drug delivery, medical imaging and cancer treatment. BacteriaBot, the bacteria-based bio-hybrid swimming microrobot, is constructed by interfacing an ensemble of live engineered bacteria with spherical and non-spherical polystyrene microparticles. BacteriaBots are envisioned to facilitate efficient transport and delivery of a wide variety of cargos for therapeutic and environmental monitoring applications.

The main goal of this dissertation was to fabricate and characterize a new generation of bacteria-assisted delivery systems featuring enhanced transport properties with the potential to efficiently deliver micro/nanoscale cargoes to desired targets and execute pre-programmed multi-agent coordinated tasks upon their arrival at the destination utilizing bacterial communication modules. BacteriaBots comprising of engineered bacteria harboring synthetic plasmids for on-board control and communication, coupled with non-spherical polymeric particles can serve as a steppingstone towards realization of intelligent drug delivery vehicles powered by bacteria and can potentially revolutionize the field of drug delivery. This dissertation is centered on three main objectives:

(1) Characterizing the transport behavior of non-spherical BacteriaBots in an isotropic environment

- Fabricating a new generation of BacteriaBots with non-spherical body shapes- bullet, barrel and prolate spheroid.
- Developing a 2D particle tracking algorithm for measurement of motility parameters of speed and directionality.
- Theoretical and experimental investigation of the effect of body shape on BacteriaBot speed and directionality.

(2) Investigating the competing roles of physical cues (i.e. body shape) and chemical cues (i.e. bacterial chemotaxis) on BacteriaBot transport

- Fabricating elliptical disk-shaped BacteriaBots.
- Studying chemotactic behavior of BacteriaBots in response to spatially variant but temporally constant gradients of a chemoattractant.

(3) Developing and characterizing a communicative network of bacteria/BacteriaBots

- Developing a microfluidic gradient generator for high-throughput characterization of bacterial/BacteriaBot quorum-sensing response.
- High-throughput characterization of the quorum-sensing response of a model bioreporter (*Escherichia coli* bacteria containing the signal-receiving component of the QS regulatory system from *Vibrio fischeri*) to a wide range of concentrations of exogenous signaling molecules.
- Characterizing the QS response of the bacteria attached onto the BacteriaBots and comparing the results with those from the bacteria-only experiments.
- Computational modeling of the QS response of a signal receiving-only bioreporter in the presence of exogenous autoinducer molecules.
- Characterizing the QS response of a chemotactic population of receiver *E. coli* in the presence of signaling molecules produced by sender bacteria in a flow-free hydrogel-based microfluidic device.

1.2 Background

1.2.1 Non-spherical polymeric particles for drug delivery applications

Micro/nanoparticles capable of carrying and delivering therapeutic and diagnostic agents to specific biological targets have exhibited improved targeting, lowered clearance and systemic toxicity, and the potential for delivering large dosages of drugs compared with conventional strategies [11]. Size and shape are among the critical properties of micro/nanoparticles which can be optimized for improving the efficacy of particle-based targeted drug delivery and diagnostic imaging. However, the biological effects of particle shape are less well understood compared with that of particle size [11]. Non-spherical particles have shown increased particle targeting [12], and also increased accumulation and retention in cancerous tumor tissues *in-vivo* [13, 14], when compared with spherical particles, verifying the significance of testing different particle shapes. In another recent study, cylindrical filomicelles have revealed persistent blood circulation for up to one week after intravenous injection which is a significant advantage over their spherical counterparts [15]. Furthermore, cellular internalization of hydrogel rod-shaped particles into HeLa cells has been investigated to better highlight the impact of using non-spherical particles on the efficiency of drug delivery [16]. To date, most of the non-spherical polymeric nanoparticles with various controllable sizes used for biomedical applications have been fabricated using bottom-up chemistry techniques [11]. However, due to the limitations of bottom-up methods for producing non-spherical particles, low-cost top-down engineering techniques such as elastic stretching of spherical particles have also been used for manufacturing such polymeric particles. The unique feature of the elastic stretching technique, and most of the other top-down methods, is the ability to independently control size, shape and chemical composition of the particles. Over 20 distinct shapes of polystyrene particles varying from 60 nm

to 30 μm in size have been recently manufactured using such technique [17], which was inspired by another work that had previously reported creating ellipsoidal PS particles [18]. Although only routine laboratory chemicals and equipment are needed for this fabrication process, a diverse range of particle geometries can be fabricated.

1.2.2 Bacteria-based drug delivery systems for cancer treatment applications

Nanoparticles with their unique physical properties including the large surface-to-volume ratio as well as tunable size, shape and surface characteristics are able to carry and deliver small molecules of DNA, RNA and proteins to the disease site with high efficiency through systemic and local administration routes [19]. Lowered clearance and systemic toxicity, higher loading capacity, better recognition of biological targets, and the ability to play a multi-functional role by simultaneously transporting multiple modalities, make nanoparticles a more efficacious route for delivering theranostics as compared to systemic administration of drug molecules and imaging agents [11, 20-24]. However, current particulate drug delivery approaches continue to rely on passive mechanisms to control the transport of drugs as well as semi-passive means to control selectivity in targeting and release rates. Although the enhanced permeability and retention (EPR) effect [25] helps deliver chemotherapeutic agents to vascularized regions of the tumor, the tumor cells in the poorly vascularized parts may not receive the cytotoxic drug in appropriate dosages. Therefore, engineered nanoparticles that are responsive to light, heat, magnetic fields or ultrasonic waves may be more efficacious in terms of covering the entire tumor microenvironment when remotely triggered [26, 27]. Alternatively, attenuated and non-pathogenic strains of bacteria have been reported to actively target diseased sites [28-30], self-propel interstitially, and successfully transfer plasmid DNA into mammalian cells [31]. This has

led to attempts for the use of bacteria as therapeutic vectors for gene therapy and cancer treatment [32]. Bacteria can specifically target tumors, however the route they take is still unknown, navigate autonomously in the presence of interstitial fluid pressure (IFP), penetrate deep in the tumor tissue and colonize the hypoxic micro-regions of the heterogeneous tumor microenvironment [33, 34]. Tumor colonization and intratumroal migration of bacteria seems to be a passive mechanism influenced by the reticuloendothelial system of the host, the tumor microenvironment and bacterial metabolism [33]. In several phase I clinical trials, an attenuated strain of *Salmonella enterica* serovar Typhimurium has revealed a good safety profile in cancer patients [35, 36]. Nonetheless, the potential immunogenicity of attenuated bacteria must be thoroughly examined before their widespread use in clinical settings. Bacteria-based drug delivery vehicles including recombinant bacteria, bacterial ghosts and bio-hybrid systems are envisioned to considerably improve targeted drug delivery and diagnostic imaging [37]. Bio-hybrid systems are comprised of two subunits: bacteria as targeting drug delivery agents and micro/nanoparticles as efficient and selective carriers of therapeutic and/or imaging agents. In contrast to utilizing only bacteria as the cargo carrier agent, invasive properties of bacteria in bio-hybrid systems enhances delivery efficiency of micro/nanoparticles without the need for genetic manipulations of bacteria for different cargos [31]. Bio-hybrid drug delivery systems are expected to offer unique benefits such as reduced required drug dosage due to enhanced targeting and transport of drug nanoparticles by bacteria. These attributes are particularly favored in targeted drug delivery with large extravascular traveling distances in primary solid tumors. We have developed a wide variety of bacteria-based bio-hybrid delivery systems, called BacteriaBots, using different bacterial species and different sizes and shapes of polystyrene

particles. Three representative generations of BacteriaBots with *Serratia marcescens*, *E. coli*, and *S.* Typhimurium have been depicted in Fig. 1.1.

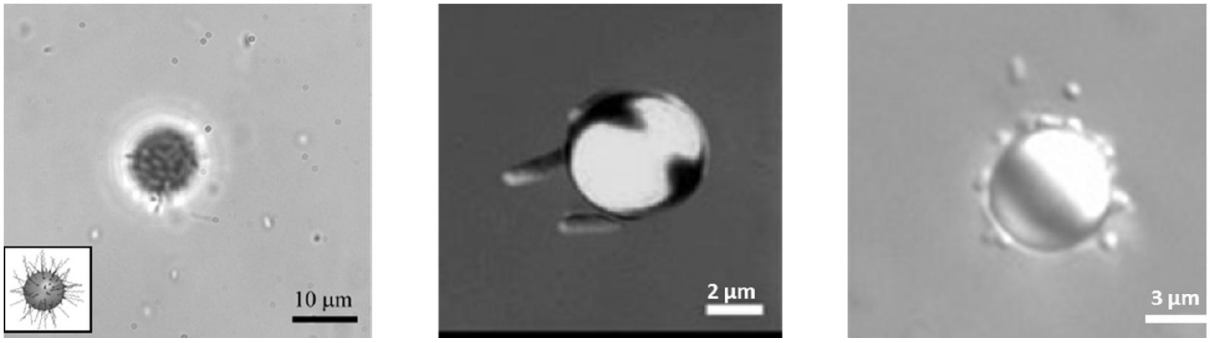

Figure 1.1 Bacteria carrying particles in the form of a bio-hybrid system (i.e. BacteriaBots); (a) *Serratia marcescens* [38], (b) *Escherichia coli*, and (c) *Salmonella* Typhimurium carrying micron-sized polystyrene particles.

1.2.3 Cell-cell communication through diffusible signals

Many bacterial species produce, release and respond to signaling molecules, called autoinducers, in order to effectively communicate information with each other and/or monitor the transport properties of their immediate environment through a process termed quorum sensing (QS) [39]. This process occurs not only within the world of microorganisms [40], but also in the mutual interactions of prokaryotic and eukaryotic cells [41] where each autoinducer structure can be recognized by the same or sometimes other bacterial species (or eukaryotic cells) and trigger expression of target genes, if a critical concentration of the autoinducers is reached [42]. This signal transduction enables the bacteria to coordinate group activities such as light production, pathogenesis and virulence, sporulation, swarming motility and biofilm formation [43-49]. Acyl-

homoserine lactone (AHL)-mediated systems, which are present in many Gram-negative proteobacteria, are the simplest QS paradigm. Specifically, the canonical LuxI/LuxR family falls in the category of AHL-based communication systems in which AHL is produced by LuxI autoinducer synthase and released in the extracellular environment. At a critical AHL concentration, the autoinducer molecule binds specifically to the LuxR regulatory protein and this complex regulates downstream genes upon binding to the *lux* box region [39]. The typical example of Gram-negative proteobacteria containing a LuxI/LuxR network is the marine bacterium, *Vibrio fischeri*, which has all the genes required for monitoring its population density and activating expression of luminescence genes through production of the autoinducer, N-(3-oxo-hexanoyl)-L-homoserine lactone (3-oxo-C6-HSL) [50]. In this regulatory system, shown in Fig. 1.2 (a), 3-oxo-C6-HSL is produced by LuxI autoinducer synthase and the 3-oxo-C6-HSL-LuxR complex interacts with the promoter region of the *lux* operon leading to transcription of bioluminescence genes [51]. Bioluminescence of *V. fischeri* was first observed in culture flasks in laboratory [47, 52] and later, the role of the same bacteria in colonizing the light organs of marine animals as part of a symbiotic relationship was investigated (see Fig. 1.2 (b) for two examples of QS in nature) [42].

Synthetic biology has provided the tools for modulating existing biological network and/or constructing recombinant plasmids to enable the host cells to perform novel tasks in addition to their native cellular processes [53, 54]. More specifically, synthetic biological circuits are designed and applied to bacterial cells aiming at programming desired phenotypes such as QS within bacterial communities [55]. For example, the transfer of the whole or a part of the LuxIR genetic system from *V. fischeri* to *E. coli* bacteria has programmed the transformed bacteria to acquire QS-induced motility switch [56], biofilm formation [57], programmed population control

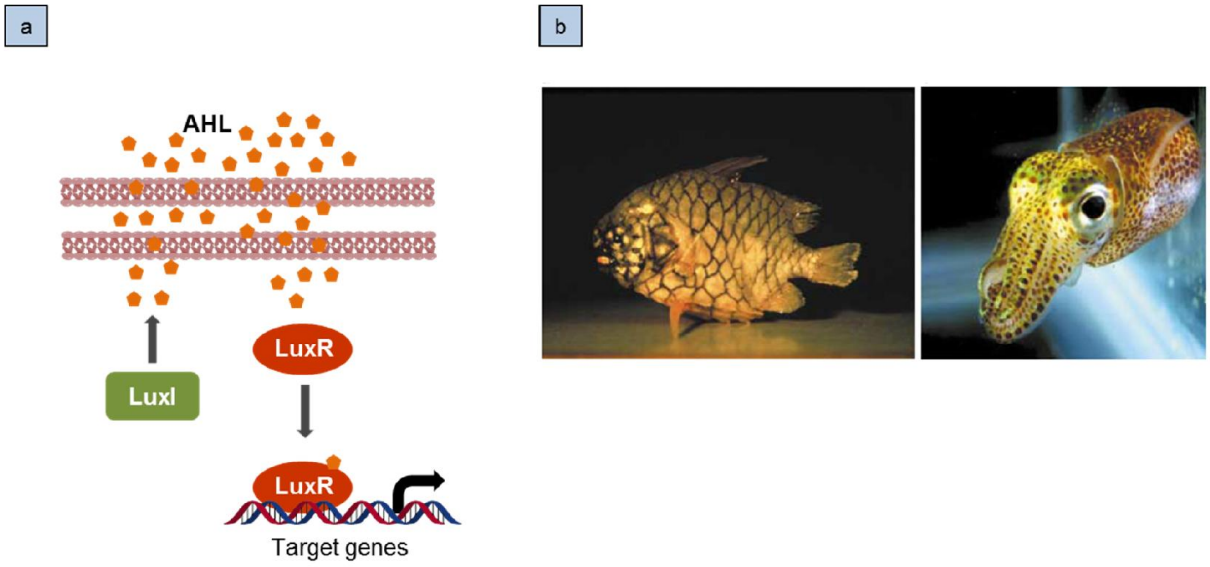

Figure 1.2 (a) The LuxIR network in *Vibrio fischeri.* AHL molecules are produced, released and taken up by the bacterium. (b) Bioluminescence of *Vibrio fischeri* in the light organs of marine animal [42].

via regulated killing of cells [58], pattern formation [59] and invasion of cancer cells [60]. If *E. coli* is transformed with the response elements including *luxR* and promoter P_{luxI}, this receiver-only circuit ($LuxI^-$) lacks the ability to synthesize AHL but allows for green fluorescent protein (GFP) expression when AHL concentration is within a certain range [59]. The cooperative QS behavior of bacteria can be exploited for generating a mobile network of bio-hybrid systems including the BacteriaBots. Engineered BacteriaBots are envisioned to execute collaborative theranostic tasks at targeted disease sites by harnessing the chemical signaling of the surface-attached bacteria.

1.3 Organization of the dissertation

The main goal of this dissertation is to fabricate, assemble, and characterize different components of a mobile network of BacteriaBots envisioned mainly for drug delivery applications and also to characterize the transport and communication of such bacteria-based systems. To reach this goal, the body of the BacteriaBots (i.e. polymeric microparticles) was engineered to improve their transport characteristics and the attached motile bacteria were imparted with new biological parts to enable the BacteriaBots to accomplish coordinated group activities upon arrival at their destination. In this regard, the rest of this document is organized as follows:

Chapter 2: In this chapter, a collection of BacteriaBots with non-spherical geometries was fabricated to investigate the role of body geometry on self-propulsion of BacteriaBots. Utilizing a high-throughput polystyrene microparticle casting and stretching technique, non-spherical BacteriaBots were produced with *E. coli* MG1655 as the microrobot actuator. Next, the motile behavior of BacteriaBots (e.g. speed and directionality) with different body shapes of sphere, barrel, bullet and prolate spheroid was characterized using a two-dimensional particle tracking algorithm. Furthermore, the directional coefficients of drag for spherical and non-spherical geometries were compared to explain the observed enhanced directionality in non-spherical geometries. Use of non-spherical particles combined with the invasive properties of motile bacteria provides a new spectrum of solutions for designing carriers with higher efficiency for rapidly evolving nanomedicine applications.

Chapter 3: The autonomous disk-shaped BacteriaBots fabricated in this chapter are a new generation of bacteria-based cargo carriers expected to exhibit a prolonged circulation in the bloodstream, which is desirable for drug delivery purposes. The potential drug delivery agents

constructed here are comprised of motile *E. coli* MG1655 bacteria and elliptical disk-shaped microparticles to enhance transport characteristics of such bio-hybrid systems. The transport direction for these agents was controlled through biased random walk of bacteria in the presence of chemoattractant gradients in a process known as chemotaxis. A flow-free microfluidic platform was utilized to establish linear concentration gradients of chemoattractant for these bio-hybrid systems. The hydrogel-based microfluidic device used in this study created a suitable microenvironment to analyze the contributions of chemotaxis and geometry to the transport of the delivery vehicles.

Chapter 4: In this chapter, *E. coli* bacteria, which are the living element of BacteriaBots, are imparted with the AHL autoinducer receiving components of a QS regulatory system of *V. fischeri* with the aim of inducing corresponding gene expression in bacterial population and thus, controlled GFP expression in BacteriaBots population, upon reaching a threshold level for the autoinducers. Here, a microfluidic diffusive mixer was utilized to quantify the QS response of the engineered *E. coli* MG1655 bacteria in response to exogenously introduced autoinducers in a high-throughput manner. Similar microfluidic settings are used for conducting the BacteriaBot experiments and a mathematical model associated with the receiver-only bacteria was presented and simulated which can help design more meaningful experiments towards understanding the functions associated with the individual elements of the QS network.

Chapter 5: The hydrogel-based microfluidic device used earlier in Chapter 3 enables us to characterize the QS response of a chemotactic population of receiver bacteria to the signaling molecules released from the sender *E. coli* bacteria. This characterization is one more step towards completion the development of an autonomous network of bacteria-based bio-hybrid delivery vehicles.

Chapter 6: The original contributions of this Ph.D. dissertation are summarized and concluding remarks are presented in this chapter. Future directions towards completion and practice of the developed autonomous network of BacteriaBots are also addressed in this final chapter.

Chapter 2: Effect of body shape on the motile behavior of bacteria-powered swimming microrobots (BacteriaBots)*

Abstract

Swimming microrobots are envisioned to impact minimally invasive diagnosis, localized treatment of diseases, and environmental monitoring. Dynamics of micro-scale swimming robots falls in the realm of low Reynolds number, where viscous forces exerted on the robots are dominant over inertia. Viscous forces developed at the interface of the swimming microrobots and the surrounding fluid are a strong function of the body geometry. In this work, a collection of bacteria-powered micro-robots (BacteriaBots) with prolate spheroid, barrel, and bullet-shaped bodies is fabricated and the influence of body shape on the dynamics of the BacteriaBots is investigated. We have experimentally demonstrated that using non-spherical geometries increases the mean directionality of the motion of the BacteriaBots but does not significantly affect their average speed compared with their spherical counterparts. We have also demonstrated that directionality of non-spherical BacteriaBots depends on the aspect ratio of the body and for the case of prolate spheroid, a higher aspect ratio of two led to a larger directionality compared to their low aspect ratio counterparts.

*This chapter has been published in the form of a journal article: A. Sahari, D. Headen, and B. Behkam, "Effect of body shape on the motile behavior of bacteria-powered swimming microrobots (BacteriaBots)", Biomedical Microdevices, 2012; 14:999-1007.
Devon Headen contributed to this work with the design and manufacturing of the mechanical stretcher as well as fabricating spheroidal non-spherical particles. Bahareh Behkam directed this effort and contributed to the experimental planning, development of the mathematical model, and manuscript preparation.

2.1 Introduction

Mobile microrobots can travel to previously inaccessible small spaces and are envisioned to impact the field of robotics as inexpensive agents of distributed networks of swarm robotic systems. The potential applications of such micro-robots include minimally invasive diagnosis, localized treatment of diseases, and environmental monitoring [1]. With the recent advances in micro/nanofabrication and assembly methods, truly microscale robotic systems with characteristic dimensions less than 100 μm have been realized [2, 3]. However, these microrobots were actuated and controlled by an off-board magnetic field. Realization of on-board actuation along with communication and control modules are among the most significant challenges towards manufacturing microscale mobile robots with advanced functionalities. Over the past few years, bio-hybrid approaches have been widely employed as a possible solution to address these challenges by integrating live prokaryotic or eukaryotic cells within robotic systems [4-10]. The most widely used of such living cells that can be exploited as on-board actuators are motile bacterial cells with the capabilities of converting chemical energy to motion and responding to environmental stimuli. *BacteriaBot,* the bio-hybrid swimming microrobot that is the subject of this study, is constructed by interfacing an ensemble of live flagellated bacteria with spherical and non-spherical polystyrene (PS) microparticles with the ultimate purpose of using bacteria for actuation, sensing, communication, and control.

Swimming motility of flagellated bacteria is well characterized and falls under two characteristic modes of *run* and *tumble* [61]. The random run-and-tumble behavior of swimming bacteria leads to the three dimensional random walk of these microorganisms [62] and consequently to the stochastic motion of the microparticles that have bacteria attached on the surface. Bacterial random walk and consequently the motion of microparticles can be actively controlled using

different stimuli such as magnetic field, certain wavelengths of light, and chemo-attractant gradients which respectively trigger magnetotaxis, phototaxis, and chemotaxis in bacteria [4, 8, 63]. On the other hand, the physical properties (i.e. shape and size) of the PS microparticles, which are the synthetic bodies of the BacteriaBots, can be altered to control dynamics of the motion depending on the specific application envisioned for the BacteriaBots.

Micro/nanoparticles capable of carrying and delivering therapeutic and diagnostic agents to specific biological targets have exhibited improved targeting, lowered clearance and systemic toxicity, and the potential for delivering large dosages of drugs compared with conventional strategies [11]. Size and shape are among the critical properties of micro/nanoparticles which can be optimized for improving the efficacy of particle-based targeted drug delivery and diagnostic imaging. However, the biological effects of particle shape are less well understood compared with that of the particle size [11]. Non-spherical particles have shown increased particle targeting [12], and also increased accumulation and retention in cancerous tumor tissues *in-vivo* [13, 14] when compared with spherical particles, verifying the significance of testing different particle shapes. In another recent study, cylindrical filomicelles have revealed persistent blood circulation for up to one week after intravenous injection which is a significant advantage over their spherical counterparts [15]. Furthermore, cellular internalization of hydrogel rod-shaped particles into HeLa cells has been investigated to better highlight the impact of using non-spherical particles on the efficiency of drug delivery [16]. To date, most of the non-spherical polymeric nanoparticles with various controllable sizes used for biomedical applications have been fabricated using bottom-up chemistry techniques [11]. However, due to the limitations of bottom-up methods for producing non-spherical particles, low-cost top-down engineering techniques such as elastic stretching of spherical particles have also been used for manufacturing

such polymeric particles. The unique feature of the elastic stretching technique, and most of the other top-down methods, is the ability to independently control size, shape and chemical composition of the particles [11]. Over 20 distinct shapes of polystyrene particles varying from 60 nm to 30 μm in size have been recently manufactured using such technique [17] which was inspired by another work that had previously reported creating ellipsoidal PS particles [18]. Although only routine laboratory chemicals and equipment are needed for this fabrication process, a diverse range of particle geometries can be fabricated. We have fabricated a group of non-spherical geometries using this stretching technique and bacteria were attached to the surface of these engineered particles using a controlled self-assembly method to complete the fabrication of BacteriaBots which can be exploited for different biomedical and environmental applications.

Micro/nanoparticles coupled with bacteria can be used to efficiently deliver genes and proteins into mammalian cells for therapeutic and monitoring applications [31]. As described earlier in this section, micro/nanoparticles can be used as imaging agents or as carriers of drug molecules, and bacteria with their invasive properties are known to have the potential to penetrate mammalian cells and transfer DNA-based drug molecules into these cells through a process called 'bactofection' [32]. In this regard, *Listeria monocytogenes* has been reported to successfully transfer genetic materials into some specific mammalian cells [64]. Some other earlier case studies have offered using attenuated bacteria such as *S.* Typhimurium [64, 65] and *Shigella* [66] as delivery agents of DNA-based vaccines. In addition to playing the role of non-viral gene delivery vehicles, attenuated strains of *E. coli , S.* Typhimurium, *Vibrio cholera* and *L. monocytogenes* have the potential to survive and replicate in tumors for weeks without causing bacteremia and can significantly improve visualization of tumors utilizing light-emitting proteins

[31, 67]. Understandably there are safety concerns associated with attenuated bacteria and the risk of reversion to virulence. However, several studies thus far have demonstrated lack of substantial pathogenicity or toxicity of attenuated bacteria [68]. Most notably, *S.* Typhimurium has demonstrated a good safety profile in several phase I clinical trials in patients with cancer [35, 36].

Since micro/nanoparticles are able to transport plasmid DNA efficiently and bacteria can play the role of targeted delivery agents, a hybrid of these two will advance the current strategies for drug delivery, medical imaging and cancer treatment. BacteriaBots with *E. coli* cells attached to non-spherical geometries, as introduced in this work, can serve as a steppingstone towards realization of intelligent drug carriers powered by bacteria and potentially revolutionize the field of drug delivery. The work presented here focuses on investigating the effect of the microparticle shape on the propulsive behavior of BacteriaBots.

2.2 Materials and methods

2.2.1 Fabrication of non-spherical particles

A high throughput spherical particle casting and mechanical stretching under heat treatment, as illustrated by Fig. 2.1 (a) [17], was used to make non-spherical PS particles which act as the engineered synthetic bodies of the BacteriaBots. Briefly, 6 μm PS spheres (Polysciences, Warrington, PA) were first washed (centrifuged at 1700×g for 5 min) three times using a 30% isopropyl alcohol (IPA): Deionized water (DI) water solution. After the final wash, the pellet was resuspended in a 5% (wt/vol) polyvinyl alcohol (PVA): water solution to a final particle concentration of 0.02% (wt/vol). The suspension was cast to make a 35 μm thick film at room temperature overnight (~12 h). After the film set, it was cut into a square-shaped piece, mounted

on a custom-made stretcher and was uniformly stretched in one dimension to create ellipsoidal voids around the micro-spheres. The stretched film was then placed in a bath of hot mineral oil. The bath temperature and the stretching aspect ratio were changed to engineer the desired shapes for this study: bullets, barrels, and prolate spheroids (see Table 2.1). For the fabrication of prolate spheroids, 2% (wt/vol) glycerol was added to the PVA solution prior to casting to increase the plasticity of the film. After removal of the film from the hot oil bath and cooling, the deformed PS particles were released from the PVA film by dissolving the films in a 30% IPA: DI water solution at 80°C and then washed two more times using the same solution. Representative scanning electron microscopy (SEM) images of the manufactured particles are shown in Fig. 2.1 (b).

Table 2.1 Fabrication parameters for manufacturing non-spherical particles

Particle Shape	Stretching Aspect Ratio	Liquefaction Temperature (˚C)	Plasticizer (Glycerol)
Prolate Spheroid	1.2-1.3, 2.0	130	Yes
Barrel	1.1-1.3	130	No
Bullet	1.1-1.3	140	No

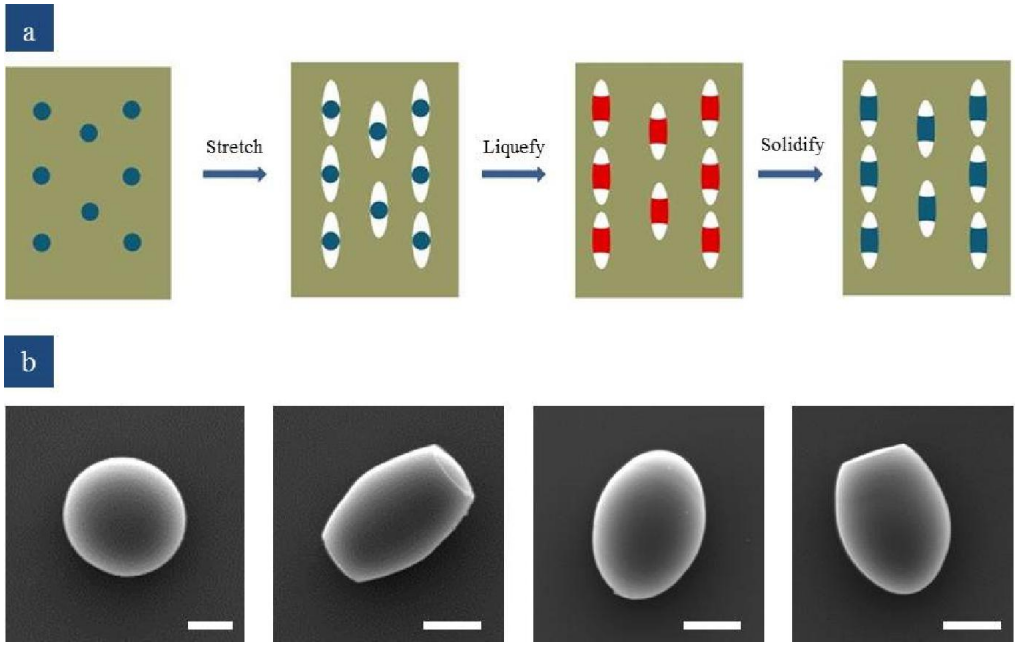

Figure 2.1 Fabrication of non-spherical polystyrene (PS) particles. (a) Step-by-step fabrication process for making non-spherical PS particles. Particles embedded in a PVA film are stretched in one dimension, liquefied in an oil bath and then solidified at room temperature; (b) Scanning electron microscopy (SEM) representative images of spherical and non-spherical PS particles. Scale bars are 2 μm.

2.2.2 Preparation of bacteria

Motile sub-populations of bacteria were isolated from the original *E. coli* MG1655 stock after an extended incubation in motility agar (1% tryptone, 0.5% NaCl, and 0.3% agar) at 30°C [69]. *E. coli* MG1655 was grown from a single colony in Luria-Bertani (LB) Broth (1% tryptone, 0.5% yeast extract, and 0.5% NaCl) in a rotary shaker incubator at 37˚C and 150 rpm. When the culture reached an optical density (OD_{600}) of 0.5, it was harvested by centrifugation at 3000×g for 5 min and the resultant pellet was resuspended in motility medium (0.01 M potassium

phosphate, 0.067 M sodium chloride, 10^{-4} M ethylenediaminetetraacetic acid (EDTA), 0.21 M glucose, and 0.002% Tween-20). The concentration of glucose in the motility medium was raised to 0.21 M from the 0.01 M used in the standard motility medium recipe [7] in order to raise the density of the medium to match that of the PS particles used in this study, enabling them to be neutrally buoyant.

2.2.3 BacteriaBot assembly

Motile *E. coli* MG1655 bacteria were interfaced with PS microparticles using Poly-$_L$-lysine (PLL, Sigma-Aldrich, St. Louis, MO). The schematic depicting the fabrication process is illustrated in Fig. 2.2. The fabricated non-spherical microparticles were added to a 0.005% (wt/vol) PLL: DI water solution and then the resulting mixture was incubated on a vortex mixer for one hour at room temperature and 500 rpm. The PLL-coated microparticles were added to the bacteria suspension allowing the bacteria to self-assemble on the BacteriaBot body. The mixture was incubated for at least 15 min at room temperature. Polydimethylsiloxane (PDMS, Sylgard 184, Dow Corning, Midland, MI) was used for making imaging enclosures required for optical microscopy. PDMS was prepared according to the manufacturer's instructions; poured in a petri dish, degassed for 10 min and finally cured at 65˚C for 4 hours. A square frame of the cured PDMS along with a clean glass slide were treated with air plasma (200 mTor, 18 W, 30 sec) in a plasma cleaner (Harrick Plasma, Ithaca, NY). The plasma treated PDMS was bonded to the treated glass slide and approximately 100 µl of the BacteriaBot sample was transferred inside the PDMS enclosure. The enclosure was sealed by placing a coverslip on top.

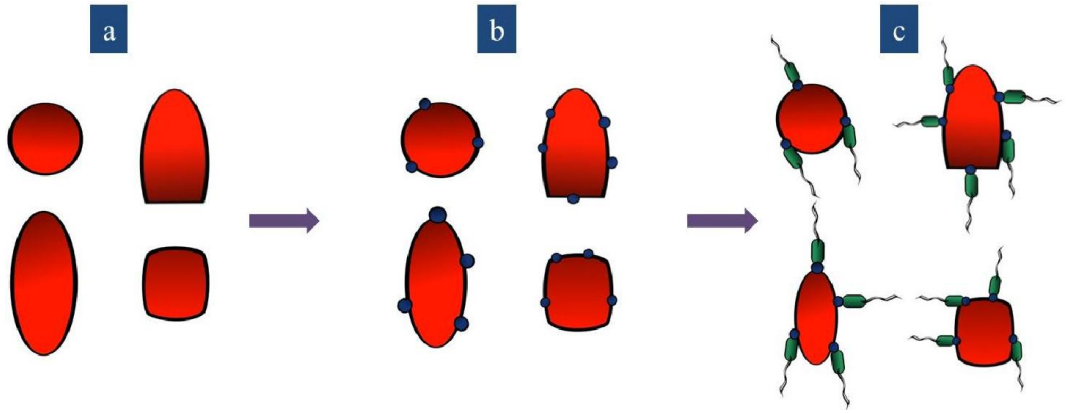

Figure 2.2 General steps in constructing BacteriaBots. a) A group of microparticles with different shapes are selected for the body of the BacteriaBots. b) The surfaces of the particles are coated with Poly-L-lysine (PLL). c) Bacteria are attached on the surface of the microparticles via controlled self-assembly.

2.2.4 Two-dimensional particle tracking

The motion of the BacteriaBots was captured for 25 seconds at 20 frames per second using a Zeiss AxioObserver D1 inverted microscope equipped with an AxioCam HSm camera. The videos were analyzed using a two-dimensional (2D) particle tracking routine developed in MATLAB (MathWorks, Natick, MA). The images were turned into binary images using a grayscale threshold and the artifacts and noises existing in most of the captured images were removed in order to distinguish the particles of interest from other objects based on differences in size. Using a border following algorithm, boundary and consequently position of each individual BacteriaBot was obtained. The nearest-neighbor method was used to link BacteriaBots in successive frames and generate their trajectories. Critical motility parameters of total distance, overall displacement, average speed, and average directionality were computed. The total distance traveled by the BacteriaBot is a measure of the total length traveled from the start to the

end of an experiment and is expressed as, distance= $\sum_{i=1}^{N}\left\|\Delta\vec{r}_{particle,i}\right\|$. N represents the total number of time steps which was equal to 500 for all the analyzed movies. The overall displacement is a measure of the length of the vector that connects the start point to the end point of the BacteriaBot motion path and is expressed as, displacement= $\left\|\vec{r}_{end}-\vec{r}_{start}\right\|$. The average speed was computed by averaging the ratio of the distance traveled by the BacteriaBot during a time step to the duration of the time step and is expressed as, average speed= $\frac{\sum_{i=1}^{N}\left\|\Delta\vec{r}_{particle,i}\right\|}{t}$. Lastly, directionality is defined as the ratio of the magnitude of the displacement vector to the total distance traveled by each BacteriaBot and is expressed as, directionality= $\frac{\left\|\vec{r}_{end}-\vec{r}_{start}\right\|}{\sum_{i=1}^{N}\left\|\Delta\vec{r}_{particle,i}\right\|}$.

2.2.5 Statistical analysis

Data were analyzed by using one-way analysis of variance (ANOVA) and $P<0.0001$ was considered as significant. Depending on the type of the data as specified below, either parametric or non-parametric one-way ANOVA was used for data analysis.

2.3 Results and discussion

While both micron-sized and nano-sized particles are currently used for therapy and diagnostics, they exhibit different responses and efficiencies in different targeted drug delivery cases. For example, microparticles have been specifically used for passive targeting to antigen presenting

cells taking advantage of the specific cellular uptake mechanisms present at the target site for these sizes of particles. Herein, we worked with microparticles (6 μm in diameter), which act as the synthetic body of the BacteriaBots. Three non-spherical geometries were fabricated here using the PS micro-sphere casting and mechanical stretching method described earlier (see 2.2.1). The critical parameters identifying the final shape of the particles include the material properties of the particle and that of the cast film (glass transition temperature and viscosity), the adhesion strength between the particle and the film, and also the film stretching extent and dimensionality [17]. Barrels, bullets and prolate spheroids were fabricated and used in the motility experiments along with spheres. After fabricating the body of the robots, BacteriaBots were constructed using PLL as a link between the *E. coli* MG1655 cells and the PS microparticles. The motility experiments were performed at room temperature and the motion of BacteriaBots was monitored over 25 second intervals at 20 frames per second using optical microscopy. Representative images of the BacteriaBots are shown in Fig. 2.3.

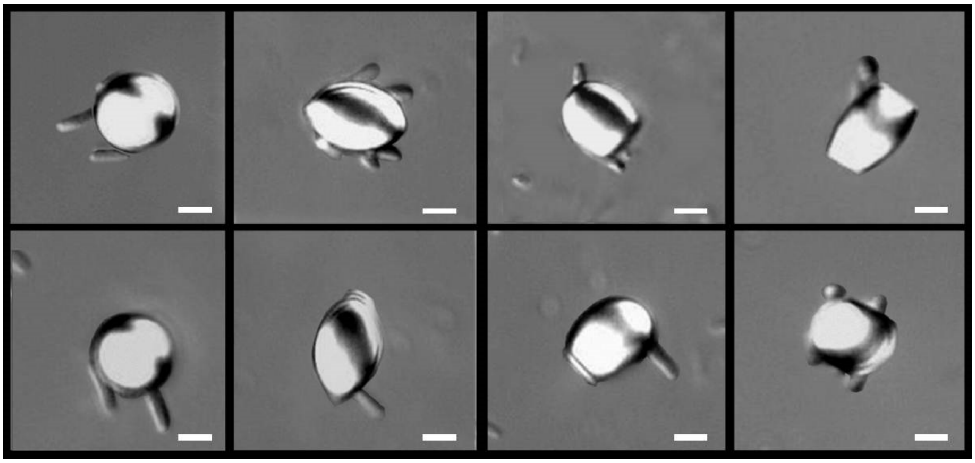

Figure 2.3 BacteriaBots with different body geometries and different numbers of attached bacteria. Each individual representative image gives a snapshot of a fabricated geometry with one or more bacteria attached on the surface. All scale bars are 2 μm.

A custom 2D image tracking routine developed in MATLAB (see 2.2.4) was utilized to characterize the motion of the BacteriaBots.

2.3.1 Theoretical analysis

The analytical expression for the mean-square displacement (MSD) of a freely rotating self-propelled spherical particle moving in three dimensions with three translational and two rotational degrees of freedom is given by [70]:

$$\left\langle \left(\vec{r}(t) - \vec{r}_0 \right)^2 \right\rangle = 8R^2 D_r t + \frac{1}{2}\left(\frac{4}{3}\beta F R^2 \right)^2 \left[2D_r t - 1 + e^{-2D_r t} \right] \qquad (2\text{-}1)$$

where r_0 is the initial position of the particle, r(t) is the position of the particle at time t, R is the radius of the particle, and F is the magnitude of the effective driving force. β and D_r are respectively defined as:

$$\beta = \left(k_B T \right)^{-1} \qquad (2\text{-}2)$$

$$D_r = \frac{k_B T}{8\pi\eta R^3} \qquad (2\text{-}3)$$

Here, k_B is the Boltzmann constant, T is the temperature, and η is the fluid dynamic viscosity.

The equivalent MSD for a freely rotating self-propelled spheroidal particle can be described by the equation given in [70]:

$$\left\langle \left(\vec{r}(t) - \vec{r}_0 \right)^2 \right\rangle = 6\overline{D}t - \Delta D t + \frac{1}{2}\left(\beta F \frac{D_a}{D_\theta} \right)^2 \left[2D_\theta t - 1 + e^{-2D_\theta t} \right] \qquad (2\text{-}4)$$

where $\overline{D} = \frac{1}{2}(D_a + D_b)$ and $\Delta D = D_a - D_b$. For a prolate spheroid with major axes of 2a and 2b, the anisotropic translational diffusion coefficients along the long axis and short axis are respectively described by [71]: $D_a = \frac{k_B T}{\gamma_a}$ and $D_b = \frac{k_B T}{\gamma_b}$. The rotational diffusion coefficient of the prolate spheroid about its short axes is: $D_\theta = \frac{k_B T}{\gamma_\theta}$, where γ_a, γ_b, and γ_θ are the translational and rotational coefficients of drag, defined as: $\gamma_a = 6\pi\eta b G_a$, $\gamma_b = 6\pi\eta b G_b$, and $\gamma_\theta = 6\eta V G_\theta$.

V is the volume of the spheroid and G_a, G_b, and G_θ are geometric factors analytically derived from the Perrin's equations [72]. For ϕ>1:

$$G_a = \frac{8}{3}\frac{1}{\left[\frac{2\phi}{1-\phi^2} + \frac{2\phi^2-1}{(\phi^2-1)^{3/2}}\ln\left(\frac{\phi+\sqrt{\phi^2-1}}{\phi-\sqrt{\phi^2-1}}\right)\right]} \quad (2\text{-}5)$$

$$G_b = \frac{8}{3}\frac{1}{\left[\frac{\phi}{\phi^2-1} + \frac{2\phi^2-3}{(\phi^2-1)^{3/2}}\ln\left(\phi+\sqrt{\phi^2-1}\right)\right]} \quad (2\text{-}6)$$

$$G_\theta = \frac{2}{3}\frac{1}{\phi\left[\frac{2\phi^2-1}{\sqrt{\phi^2-1}}\ln\left(\phi+\sqrt{\phi^2-1}\right) - \phi\right]} \quad (2\text{-}7)$$

Here, $\phi = \frac{a}{b}$ is the aspect ratio of the spheroid.

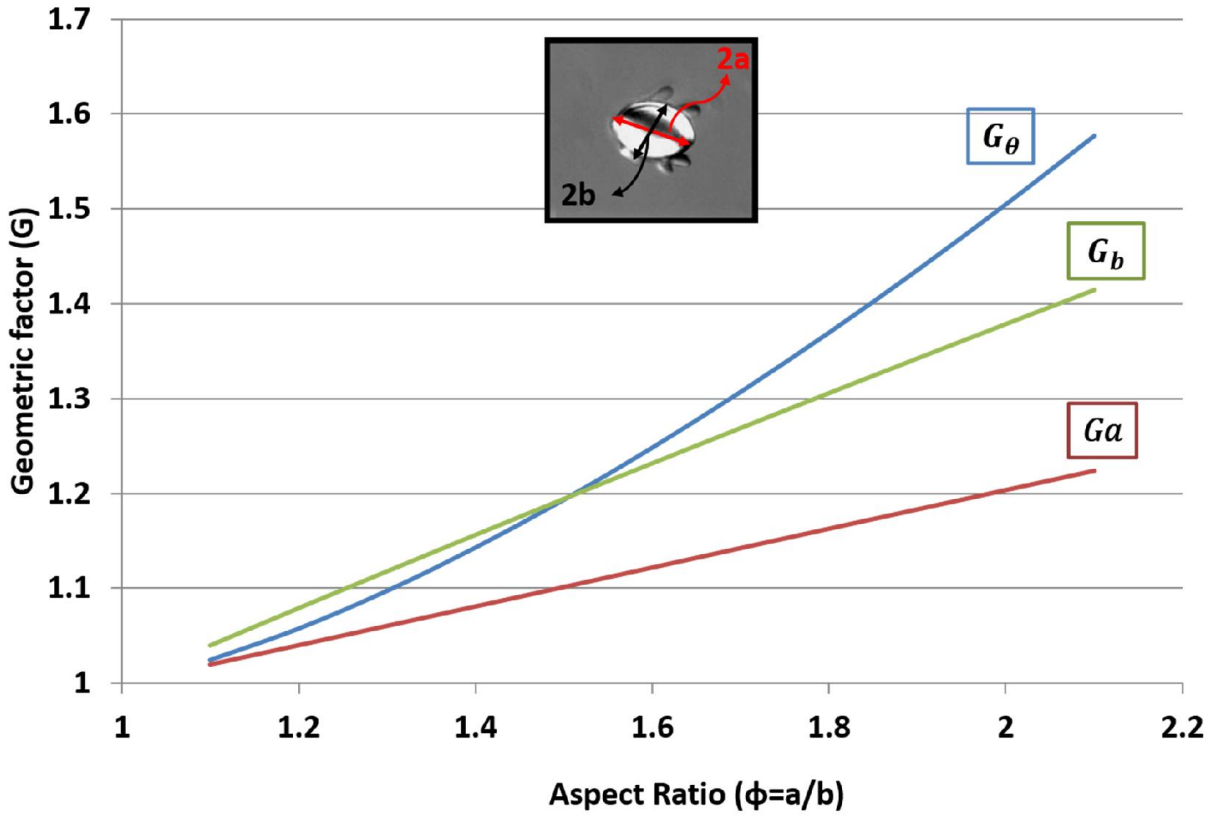

Figure 2.4 The geometric factors G for a prolate spheroid with major and minor axes lengths of 2a and 2b as a function of aspect ratio.

Equations (2-1) and (2-2) show that the motile behavior of both spheroidal and spherical self-propelled particles is a function of their respective translational and rotational coefficients of drag. These coefficients strongly depend on the geometric factors of G_a, G_b, and G_θ. Fig. 2.4 shows the variations of these geometrical factors as a function of the aspect ratio. For $\phi = 1$ (spheres), $G_a = G_b = G_\theta$. For $\phi > 1$, the differences between G_a, G_b, and G_θ are more pronounced and they continue to grow as the aspect ratio values increase. Therefore, non-spherical particles experience two directionally different translational coefficients of drag and an

increased rotational coefficient drag which results in more directional motion path for prolate spheroids compared to spheres.

2.3.2 Effect of body shape on directionality

It is of particular interest for drug delivery applications to investigate the effect of body shape on the directionality of the motion of the BacteriaBots without active steering. The average directionality of the examined BacteriaBots with different body shapes of sphere, barrel, bullet, and prolate spheroid were 0.2 ± 0.1, 0.3 ± 0.1, 0.3 ± 0.1, and 0.3 ± 0.1 respectively (see Fig. 2.5 (a)). Using non-parametric one-way ANOVA, it was concluded that the non-spherical BacteriaBots moved with a higher degree of directionality compared to their spherical counterparts ($n=15$, $P<0.0001$). Also, we found no statistically significant difference among the average directionalities of the non-spherical BacteriaBots with aspect ratios less than 1.4±0.2. The improvement in the directionality of the motion for non-spherical particles is attributed to high resistance to rotation around any of the short principal axes for the elongated non-spherical geometries. The rotation of spherical BacteriaBots about its axes of symmetry does not encounter the same resistance when compared to the rotation about the short principal axes of the non-spherical geometries (see 2.3.1). This leads to a more restricted and hence more directional motion for non-spherical BacteriaBots.

To further illustrate the dependency of directionality on the aspect ratio of non-spherical particles, prolate spheroid-shaped BacteriaBots with aspect ratios of 2.0±0.1 were tested and a larger average directionality of 0.5±0.2 was observed (See Fig. 2.5 (a)). The enhancement in the directionality of the high aspect ratio prolate spheroids is attributed to the increased differences in the coefficients of drag as shown in Fig. 2.4.

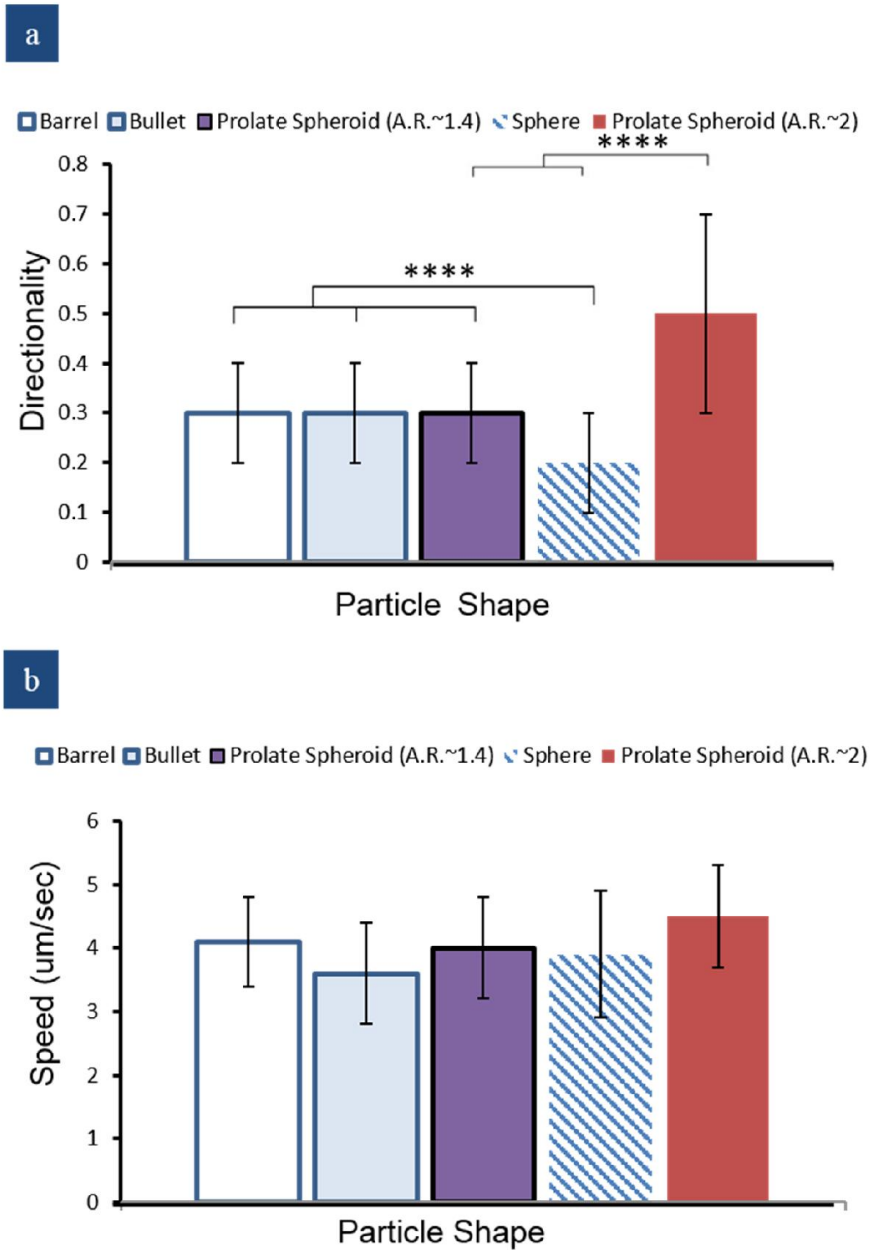

Figure 2.5 Experimental results indicating the motile behavior of BacteriaBots with different geometries. a) The directionality values of non-spherical robots are higher than that of the spherical ones (****, $P<0.0001$) and are dependent on the robot body aspect ratio. b) There is no statistically significant difference between the average speeds the BacteriaBots with different body geometries ($\alpha=0.0001$).

2.3.3 Effect of body shape on number of the attached bacteria and propulsion speed

One-way ANOVA analysis shows that the two factors of body shape and the number of attached bacteria have no interaction with each other. The average speed of BacteriaBots was found to be independent of the shape of the BacteriaBot body for aspect ratios less than 1.4±0.2. The average speed of the BacteriaBots with different body shapes of sphere, barrel, bullet, and prolate spheroid were 3.9 ± 1.0 μm/s, 4.1 ± 0.7 μm/s, 3.6 ± 0.8 μm/s, and 4.0 ± 0.8 μm/s respectively (see Fig. 2.5 (b)). Prolate spheroids with aspect ratios of 2.0±0.1 revealed a slightly larger average speed of 4.5±0.8 μm/s, as compared to their low aspect ratio counterparts. Lack of a significant difference in speed magnitudes for the studied BacteriaBots may be due to the fact that the 2D tracking method used in this study does not capture any movement that does not lead to a change in the location of the center of mass.

Two types of control experiments were also performed for different geometries to confirm that the main cause for BacteriaBot movement is the average net force exerted by the bacteria attached to the PS microparticles. The BacteriaBot motility experiment was conducted, this time with no PLL and consequently no bacteria attached to the particles. In another control experiment, different shapes of particles were suspended in motility medium and minimal displacement of the microparticles in both experiments confirmed that the bacteria attached to the mobile microparticles are the main source of propulsion. Two representative trajectories of the BacteriaBots are shown in Fig. 2.6 (a) and Fig. 2.6 (b), in which the non-spherical BacteriaBots reveal a directional movement as they self-propel in the motility medium. A sample trajectory for a control particle has also been included to show the minimal displacements associated with the control experiments (see Fig. 2.6 (c)).

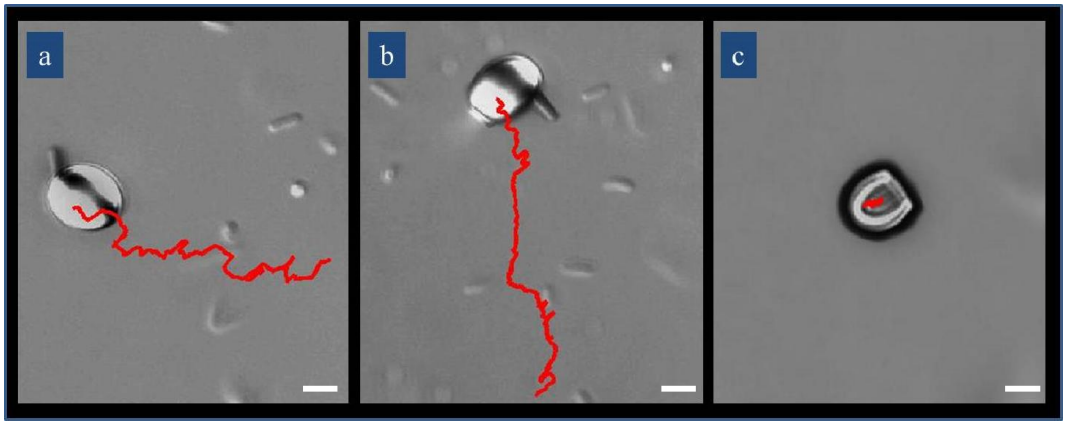

Figure 2.6 Representative trajectories of BacteriaBots. a) A prolate spheroid BacteriaBot is pushed by a single bacterium. b) A bullet-shaped BacteriaBot is pushed by a single bacterium. c) In one control experiment, the bullet-shaped particle does not displace significantly since there is no bacterium attached on the surface. All scale bars are 2 μm.

2.3.4 Effect of number of the attached bacteria on propulsion speed and directionality

Number of the attached bacteria for all body geometries varies between 1 and 6; however, as shown in Fig. 2.7-2.11, there are no correlations between the average directionality and average speed of BacteriaBots and the number of bacteria adhered on the surface (one-way ANOVA indicates no significant trend in directionality and speed of the BacteriaBots as the bacteria number changes). This can be due to the fact that based on the location of the attached bacteria relative to one another, the overall force exerted on the particle can vary. For example, if bacteria can only attach to a specific portion of the BacteriaBot surface (can be achieved through surface patterning, as demonstrated by previously [73], individual contribution of each bacterium has an appreciable effect on the dynamics of BacteriaBot and a strong dependency of the kinematic parameters such as speed on the number of bacteria is observed. However, when the entire BacteriaBot surface is available for random attachment of bacteria, there is a significantly high

probability that attached bacteria are no longer limited to a portion of the surface but rather are distributed over the entire surface of the BacteriaBot. This leads to counterbalancing of contribution of the forces of some bacteria by some others and an overall reduced force and reduced sensitivity to the number of attached bacteria, as illustrated in Fig. 2.7 (a)-2.11 (a). This is also evident by existence of a statistically insignificant dependency of the speed to the number of attached bacteria for the particle size and the range of the number of bacteria used in this study (Fig. 2.7 (b)-2.11 (b)).

In summary, the advantages of using non-spherical shapes and invasive bacteria simultaneously for biomedical applications such as diagnostic imaging and targeted drug delivery motivated us to develop a new generation of BacteriaBots. Limited particle diffusion and directional coefficient of drag are some of the attributes that are enhanced through such non-spherical BacteriaBots which can significantly help in achieving desired motion dynamics for environmental monitoring and therapeutic applications. As described earlier, bacteria are capable of exhibiting different tactic behaviors (i.e. chemotaxis, magnetotaxis, etc.) in the presence of environmental stimuli (i.e. chemical gradients, magnetic fields, etc.) depending on the species of the bacteria. In future, bacterial motile behavior will be actively controlled using such environmental factors to move BacteriaBots towards specific targets in order to accomplish a wide variety of tasks at the target site. Furthermore, other size and shape of the particles as well as bacterial species will be explored in order to design and fabricate optimal bio-hybrid vehicles for emerging applications.

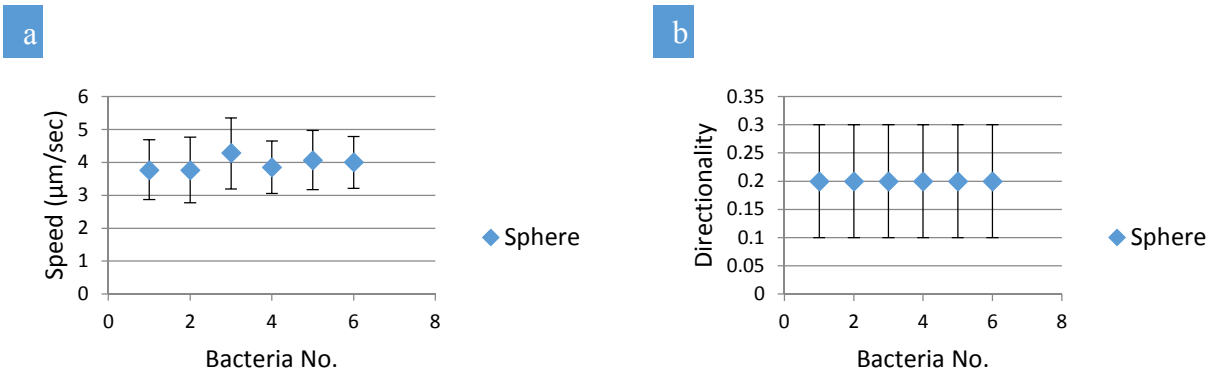

Figure 2.7 (a) Speed, and b) directionality of the spherical BacteriaBots as a function of the number of bacteria adhered on the surface of the microparticle.

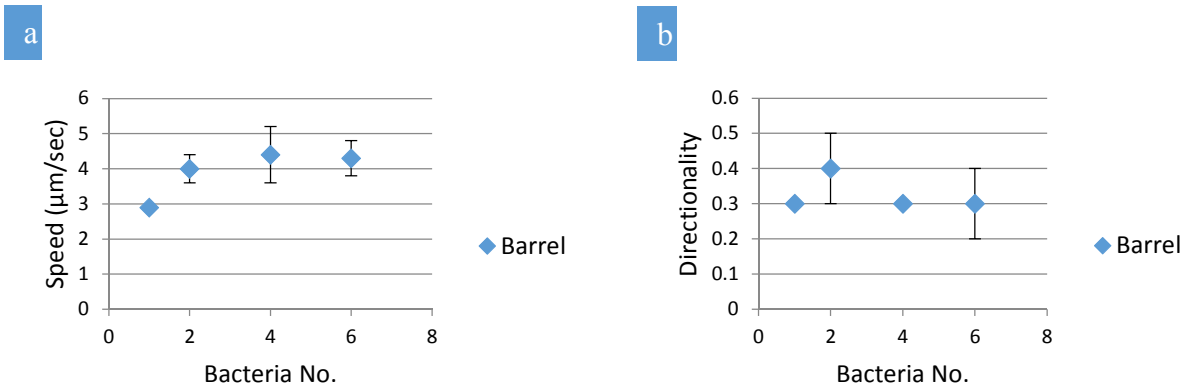

Figure 2.8 (a) Speed, and (b) directionality of the barrel-shaped BacteriaBots as a function of the number of bacteria adhered on the surface of the microparticle.

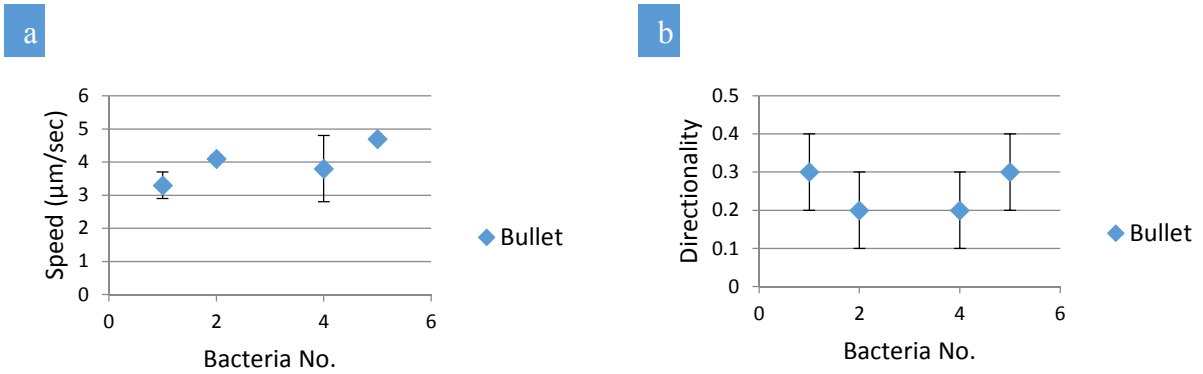

Figure 2.9 (a) Speed, and (b) directionality of the bullet-shaped BacteriaBots as a function of the number of bacteria adhered on the surface of the microparticle.

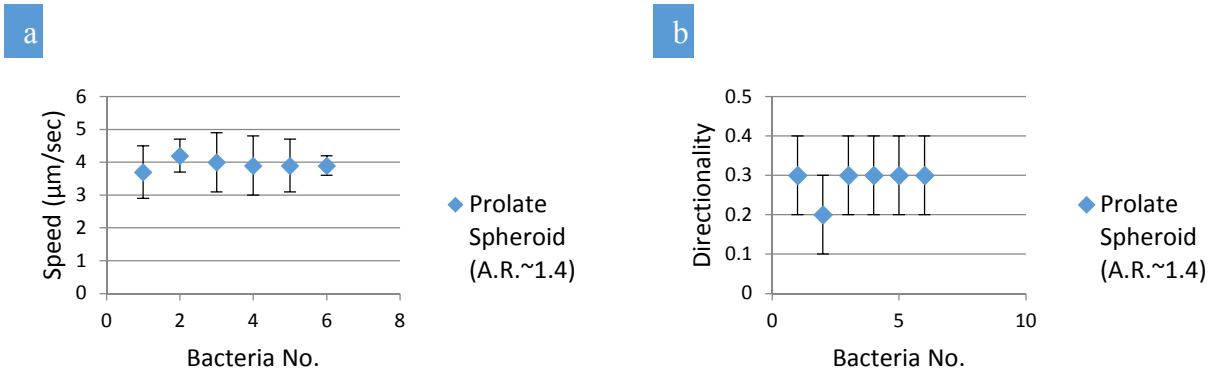

Figure 2.10 (a) Speed, and (b) directionality of the prolate spheroidal BacteriaBots (A.R. = 1.4±0.2) as a function of the number of bacteria adhered on the surface of the microparticle.

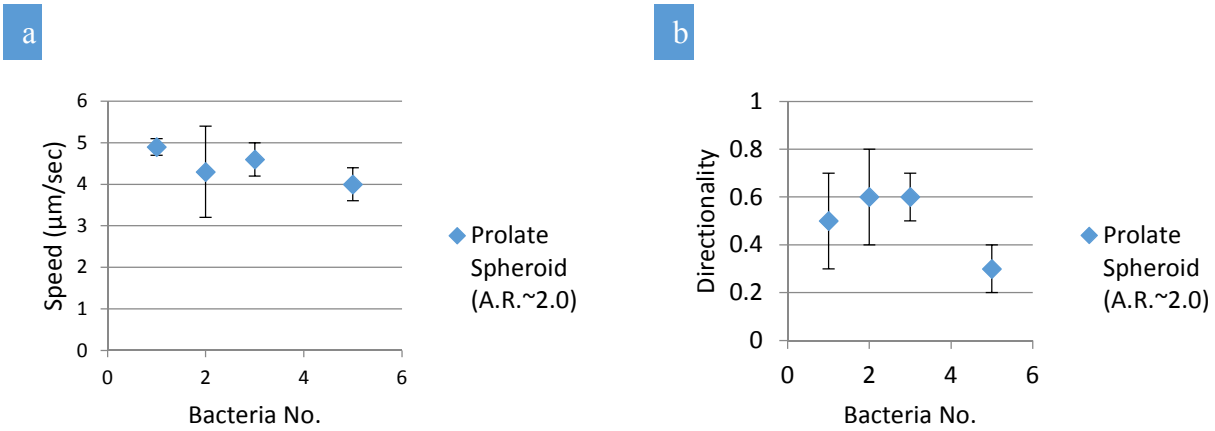

Figure 2.11 (a) Speed, and (b) directionality of the prolate spheroidal BacteriaBots (A.R .= 2.0±0.1) as a function of the number of bacteria adhered on the surface of the microparticle.

2.4 Conclusions

Particle-based drug delivery systems have had significant impact on experimental pharmaceutics and clinical medicine and bacteria with their invasive properties have the potential to guide particles towards diseased areas. Thus, bacteria and microparticles can be simultaneously used as

intelligent drug delivery agents or diagnostic imaging tools which led to fabrication of bacteria-powered micro-robots, called BacteriaBots. In this work, we designed and fabricated a collection of BacteriaBots with non-spherical geometries which can pave the way for development of optimal intelligent vehicles for therapeutic and environmental applications. Utilizing a high throughput PS microparticle manufacturing technique, we produced non-spherical BacteriaBots with *E. coli* MG1655 as the microrobot actuator. Variation in the motile behavior of BacteriaBots due to their body geometry can be very complex and can only be determined experimentally. We characterized the motile behavior of BacteriaBots with different body shapes of sphere, barrel, bullet and prolate spheroid. It was demonstrated that a non-spherical body shape improves the mean directionality of the motion and higher directionality can be achieved by increasing the aspect ratio of the robot body. Directional coefficients of drag along with the other advantages of using non-spherical particles combined with the invasive properties of motile bacteria suggest a new spectrum of solutions for designing carriers with higher efficiency for rapidly evolving nanomedicine applications.

Chapter 3: Directed Transport of Bacteria-Based Bio-Hybrid Delivery Vehicles*

Abstract

Several attenuated and non-pathogenic bacterial species have been demonstrated to actively target diseased sites and successfully deliver plasmid DNA, proteins and other therapeutic agents into mammalian cells. These disease-targeting bacteria can be employed for targeted delivery of therapeutic and imaging cargos in the form of a bio-hybrid system. The bio-hybrid drug delivery system constructed here is comprised of motile *Escherichia coli* MG1655 bacteria and elliptical disk-shaped polymeric microparticles. The transport direction for these vehicles can be controlled through biased random walk of the attached bacteria in the presence of chemoattractant gradients in a process known as chemotaxis. In this work, we utilize a flow-free microfluidic platform to establish steady linear concentration gradients of a chemoattractant and investigate the roles of chemotaxis and geometry in transport of bio-hybrid drug delivery vehicles. Our experimental results demonstrate for the first time that bacterial chemotactic response dominates the effect of body shape in extravascular transport; thus, the non-spherical system could be more favorable for drug delivery applications owing to the known benefits of using non-spherical particles for vascular transport (e.g. relatively long circulation time).

*This chapter has been published in the form of a journal article: Sahari A, Traore M. A., Scharf B. E., Behkam B. Directed transport of bacteria-based drug delivery vehicles: bacterial chemotaxis dominates particle shape. Biomedical microdevices, 2014; 16 (5):717-725.
Mahama Aziz Traore contributed to this work with the modification of the PEG-DA hydrogel-based microfluidic device that he had originally developed. Birgit E. Scharf contributed significantly to the work with the isolation and plasmid transformation of the *E. coli* MG1655m bacteria. Bahareh Behkam directed this effort and contributed to the experimental planning, data analysis, and manuscript development.

3.1 Introduction

Synthetic drug carriers including polymeric micro/nanoparticles have been developed to facilitate transport and targeted delivery of therapeutics and contrast agents to diseased sites. Lowered clearance and systemic toxicity, higher loading capacity, better recognition of biological targets, and the ability to play a multi-functional role by simultaneously transporting multiple modalities make micro/nanoparticles a more efficacious route for delivering theranostics as compared to systemic administration of drug molecules and imaging agents [11, 20-24]. However, these drug delivery approaches continue to rely on passive mechanisms to control the transport of drugs, and semi-passive means to control selectivity in targeting and release rates. In contrast, attenuated and non-pathogenic strains of bacteria have been reported to actively target diseased sites [28-30] and colonize tumors *in-vivo* [74, 75]. These disease-targeting bacteria can also be employed for targeted delivery of therapeutic and imaging cargos in the form of a bio-hybrid system [31]. We have recently developed a bio-hybrid drug delivery system, hereafter referred to as *BacteriaBots*, which is constructed by interfacing two main components: (1) spherical and non-spherical polymeric microparticles as efficient carriers of therapeutic and/or imaging agents and (2) an ensemble of live engineered non-pathogenic bacteria with the purpose of using the bacteria for active transport and targeting. Invasive properties of bacteria enhance delivery efficiency of microparticles without the need for genetic manipulations of bacteria for different cargos. Therefore, BacteriaBots are expected to offer unique benefits such as reduced required drug dosage (due to active targeting of bacteria) and enhanced interstitial transport of drug particles (due to self-propulsion of bacteria). These attributes are particularly favored in targeted drug delivery to primary solid tumors where regular

therapeutics cannot access via passive diffusion due to the existing elevated interstitial pressure and long extravascular diffusion distances.

Non-spherical micro/nanoparticles have been recognized to improve performance of targeted delivery of therapeutics and contrast agents [15, 16, 21] which makes them a good candidate for the synthetic element of a BacteriaBot. Although several species of motile flagellated bacteria have been utilized to propel microparticles of various geometries [4, 5, 7, 8, 76, 77], competing effects of body geometry (physical cues) and chemoattractant gradient (chemical cues), naturally present in physiologically relevant environments, have not been investigated. In presence of chemoattractant gradients, bacteria extend their run periods and move towards the chemoattractant source in a biased random walk process known as chemotaxis [78], which leads to the biased motility of the microparticles they are attached to [63].

In this work, Elliptical disk (ED)-shaped microparticles were fabricated using a casting and mechanical stretching technique and used as the abiotic body of the non-spherical BacteriaBots. Each BacteriaBot was constructed by conjugating a streptavidin-coated spherical or non-spherical polystyrene microparticle with a specific derivative of *E. coli* MG1655 with increased motility decorated with a biotinylated cell membrane specific antibody. This method of BacteriaBot construction takes advantage of the strong non-covalent bond between biotin and streptavidin. Using our recently reported flow-free poly(ethylene glycol) diacrylate microfluidic chemotaxis assay device [79], we established quasi-steady linear gradients of the chemoattractant, L-aspartic acid, for characterizing the chemotactic behavior of BacteriaBots with two different shapes- ED and sphere. The results from this study elucidate the transport behavior of spherical and non-spherical BacteriaBots in presence of chemical gradients and negligible flow. The non-spherical BacteriaBots developed here are envisioned to overcome the

limitations of passively targeting particulate systems through more efficient transport and delivery of cargos to diseased areas.

3.2 Materials and methods

3.2.1 BacteriaBot construction

ED-shaped polystyrene particles were fabricated using a high-throughput particle casting and mechanical stretching technique [17]. First, 6 μm carboxylate polystyrene microspheres (2.65% (w/v), Polysciences, Warrington, PA) were washed three times by centrifugation at 3,000 × g for 5 min using 30% (v/v) isopropyl alcohol (IPA) in deionized (DI) water. After the final wash, the pellet was resuspended in a 5% (w/v) polyvinyl alcohol (PVA) solution in DI water (at 90 ºC) to a final particle concentration of 0.062% (w/v). 2% (v/v) glycerol was added to the PVA/particle solution prior to casting to increase the plasticity of the film. The suspension was then cast and left at room temperature overnight (~12 h) to make a 35 μm thick film. After the film set, it was carefully cut into a square-shaped piece, mounted on a custom-made stretcher and was uniformly stretched in one dimension to a final aspect ratio of ~2. The stretched film was then immersed in a bath of toluene at room temperature for 3 hours, air-dried for 10 hours, dissolved in 30% IPA (in DI water) overnight and finally washed five more times to extract the residual toluene and purify the ED particle solution. The spherical particles, used along with the fabricated ED particles in the experiments, were 6 μm carboxylate polystyrene microspheres from the same stock solution that were washed three times by centrifugation at 3,000 × g for 5 min using 30% IPA (in DI water). Derivatives of *Escherichia coli* MG1655 with increased motility, hereafter referred to as *E. coli* MG1655m, were isolated after extended incubation on motility agar [69]. *E. coli* MG1655m, transformed with a plasmid encoding GFP (pHC60; tet^R, constitutive expression

of green fluorescent protein) [80] using standard protocols [81], was grown overnight at 32 ˚C and 150 rpm in a shaker incubator (Excella E24, New Brunswick, Edison, NJ) in 10 ml of tryptone broth (TB; 1% tryptone and 0.5% NaCl) supplemented with tetracycline (10 μg ml^{-1}) and then diluted 1:100 in TB to start a 10 ml of fresh bacterial culture in a 125 ml flask at 32 ˚C and 150 rpm. When the bacterial culture reached OD_{600} of 0.5, 1 ml of the culture was harvested by centrifugation at 1,700 × g for 5 min and the resultant pellet was resuspended in motility buffer adjusted for neutral buoyancy of BacteriaBots (0.01 M potassium phosphate, 0.067 M sodium chloride, 10^{-4} M ethylenediaminetetraacetic acid, 0.21 M glucose, and 0.002 % (v/v) Tween-20, pH=7.0). The two collections of spherical and ED particles were incubated with 5 μg ml^{-1} streptavidin-Cy3 (Sigma-Aldrich) and the bacterial suspension were treated with 1 μg ml^{-1} goat polyclonal anti-lipid A LPS antibody labeled with biotin (Thermo Scientific) both for 1 hour at room temperature and at 500 rpm on a vortex shaker. At the end of incubation period, the bacteria and microparticles suspensions were respectively centrifuged at 1,700 × g and 3,000 × g to remove unbound antibody and streptavidin-Cy3 by removing the supernatants. The bacteria were then resuspended in 1 ml motility buffer and the particles were resuspended in 400 μl motility buffer. Lastly, 100 μl from the suspension of the antibody-decorated bacteria was mixed and incubated with the streptavidin-coated particles for 30 min at room temperature and at 500 rpm to produce BacteriaBots through self-assembly and utilizing the high affinity between biotin and streptavidin. Schematics of the BacteriaBot system and its components are illustrated in Fig. 3.1 (a) and (b). An inverted fluorescence microscope with a 63 × DIC objective was used to verify co-localization of bacteria and microparticles and count the number of bacteria attached to the microparticles (Fig. 3.1 (d)).

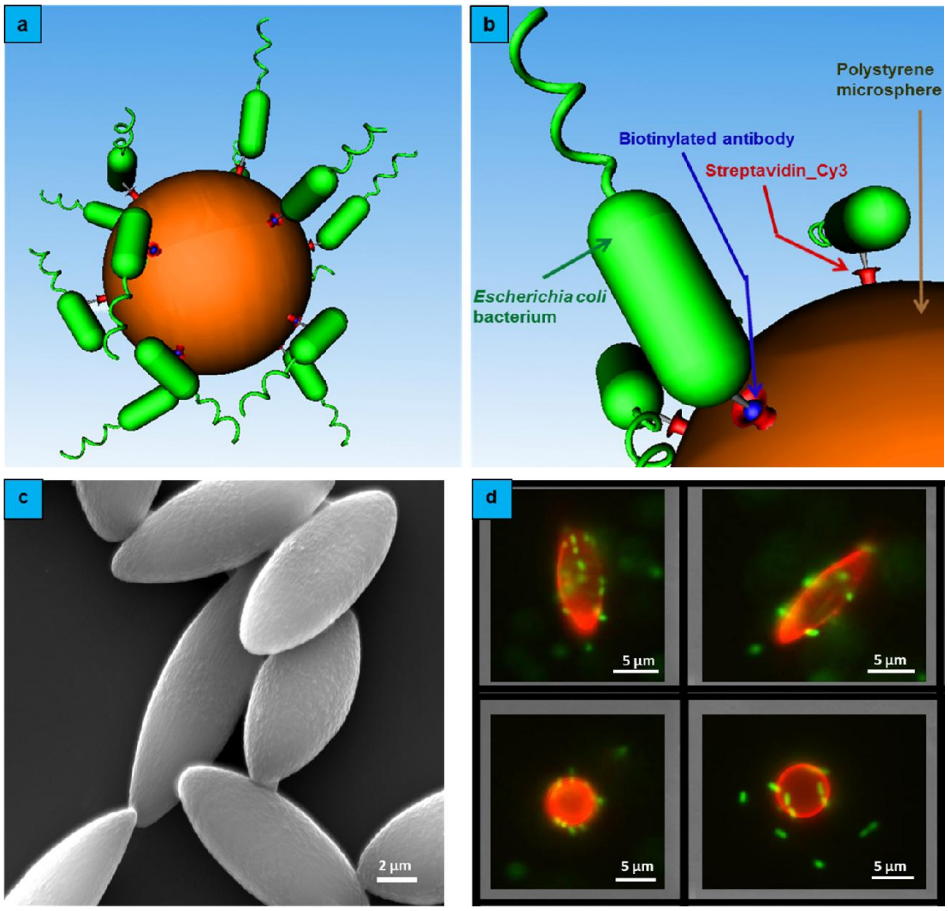

Figure 3.1 (a) Schematic of a spherical BacteriaBot; (b) Illustration of the BacteriaBot components: GFP-expressing *E. coli* bacteria are decorated with a cell membrane specific antibody labeled with biotin and then conjugated with streptavidin-Cy3 coated polystyrene microparticles taking advantage of the strong non-covalent bond between biotin and streptavidin; (c) A representative scanning electron microscopy (SEM) image of elliptical disk-shaped polystyrene particles (i.e. the body of the non-spherical BacteriaBots); (d) Representative fluorescence microscopy images of spherical and elliptical disk-shaped BacteriaBots. Co-localization of bacteria (in green) and microparticles (in red) indicates successful fabrication of the bacteria-particle conjugates.

3.2.2 Microfluidic device fabrication and assembly

We have recently reported a flow-free poly(ethylene glycol) diacrylate (PEG-DA) microfluidic chemotaxis assay device that is fabricated through a one-step photolithography process [79]. A schematic of the device is illustrated in Fig. 3.2 (a). Briefly, 10% (v/v) PEG-DA hydrogel (MW 700 Da) precursor solution in phosphate buffered saline (PBS) was mixed with 10% (w/v) Irgacure® 2959 photoinitiator solution (in 70% ethanol) at a 1:20 ratio to make the hydrogel solution. Polydimethylsiloxane (PDMS, Sylgard 184), prepared according to manufacturer's instructions, was spin-coated on a clean 1 mm glass slide to make a 300 μm thick PDMS layer. The PDMS-coated glass slide was cured on a hot plate at 100 °C for 45 min and then the PDMS was cut into a square shape frame to build an enclosure for the hydrogel solution. To ensure a good seal between the PEG-DA device and the underlying glass substrate, the enclosure was rendered hydrophilic using oxygen plasma (200 mTorr, 18 W, 5 minutes) and salinized with a 2% (v/v) mineral oil solution of 3-(trichlorosilyl) propyl methacrylate for 10 min. The glass/PDMS chip was then thoroughly rinsed with 100% ethanol and hard baked at 95 °C. The PEG-DA hydrogel solution was poured in the square PDMS enclosure on the glass slide, a glass mask was placed on top, and the hydrogel was polymerized by exposure to UV light (365 nm, 18 W/cm^2, Omnicure S1000, Vanier, Quebec) for 15 sec. The three-channel pattern transferred onto the hydrogel were 500 μm wide and spaced 500 μm apart and had the 300 μm depth of the PDMS frame. The hydrogel device was then soaked in DI water overnight to remove any excess photoinitiator. A 4 mm thick square shape PDMS layer was made in a petri dish, punched to pass the tubes through and placed directly on top of the hydrogel pattern in the PDMS frame to provide sufficient support for the hydrogel and prevent fluid leaking. Two plexiglass support layers on top and one underneath the glass slide were used to provide sufficient pressure for the

assembly of the device.The hydrogel device layer and the assembled microfluidic platform are shown in Fig. 3.2 (b) and (c), respectively.

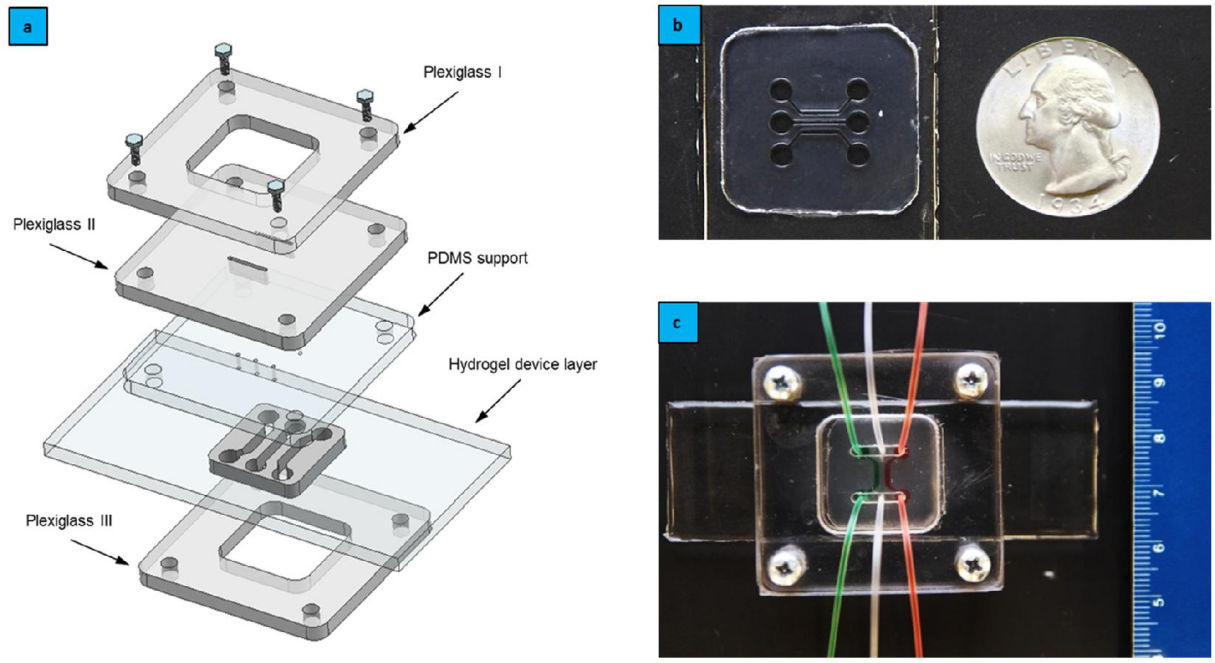

Figure 3.2 The microfluidic device at a glance; (a) Expanded view of the device comprising of the top and bottom plexiglass support layers, a third plexiglass layer for supporting the PDMS layer covering the hydrogel device layer. The hydrogel device consists of three parallel channels, each 500 µm wide and spaced 500 µm apart; (b) Photograph of the hydrogel device layer (top view) with a U.S. 25¢ coin for comparison; (c) Functional testing of the assembled microfluidic device using colored test fluids.

3.2.3 Bacteria/BacteriaBot chemotaxis assay

To eliminate the effect of fluid flow on the bacteria and BacteriaBot chemotaxis, the flow-free microfluidic device described above was used to generate quasi-steady chemical concentration gradients. L-aspartic acid, a known chemoattractant for *E. coli* K-12, at spatially varying and

temporally constant concentration gradients was used to direct the motility of bacteria and BacteriaBots. First, motility buffer solution was manually loaded in the center channel and the corresponding tube was clamped after filling up the channel to prevent any fluid flow and liquid evaporation. The gradients were established by continuously flowing the chemoattractant solution (in motility buffer) and the blank motility buffer solution in the two feeder channels at 5 μl min^{-1}, and by lateral diffusion of the chemoattractant through the hydrogel walls and into the flow-free buffer-filled center channel. L-aspartic acid gradients ranging from 1.7×10^{-6} M mm^{-1} to 1.7×10^{-3} M mm^{-1} was used to direct motility of *E. coli* MG1655m and the two concentration gradients of 1.7×10^{-5} M mm^{-1} and 1.7×10^{-4} M mm^{-1}, generated by loading the chemoattractant feeder channel respectively with 33.8 μM and 323.3 μM L-aspartic acid in motility buffer, were used to examine the effect of chemoattractant concentration gradients on transport behavior of BacteriaBots. The quasi-steady linear gradients in the center channel of the microfluidic device were maintained throughout the entire experiment. In the bacterial chemotaxis assay, *E. coli* MG1655m transformed with pHC60 was grown using the two successive culturing method described earlier. When the bacterial culture reached OD_{600} of 0.5, 1 ml of the culture was harvested by centrifugation at 1,700 × g for 5 min and the resultant pellet was resuspended in 10 ml of motility buffer. After injecting the bacterial suspension in the center channel, the bacterial spatial distribution was monitored and imaged using an inverted fluorescence microscope with a 20 × objective lens. In the BacteriaBot chemotaxis assay, 500 μl solution of BacteriaBots was loaded in a 1 ml syringe, injected into the center channel of the device replacing the blank motility buffer. After waiting for 5 min to reestablish the gradient, the BacteriaBots distribution was imaged 1500 μm downstream from the inlet of the center channel every 5 min at 20 frames per second for 10 seconds for the duration of the entire experiment using phase-contrast

microscopy and a 20 × objective lens. Negative control experiments with motility buffer flowed in both side channels were also performed to verify that the migration of BacteriaBots towards one specific side is only because of chemotaxis.

3.2.4 Data analysis

To quantify the migration profile of bacteria/BacteriaBots, the width of the observation channel was divided in two halves and the spatial distribution of the objects was calculated in each half of the channel using the ImageJ software. Chemotaxis Partition Coefficient (CPC) is a population-scale metric that was used throughout the study to analyze the effect of chemotaxis on bacterial/BacteriaBots distribution [82]:

$$CPC = \frac{(B_r - B_l)}{(B_r + B_l)} \qquad (3-1)$$

where B_r is the number of bacteria/BacteriaBots in the right half of the center channel and B_l is the number of bacteria/BacteriaBots in the left half. For the BacteriaBots chemotaxis experiment, the numbers of the mobile microrobots in both halves of the main channel were counted visually and substituted $B_i|_{i=r,l}$ to compute the corresponding CPC value. To evaluate the migration of BacteriaBots at individual scale, the captured videos were analyzed using a custom two-dimensional particle tracking routine previously developed in MATLAB (MathWorks, Natick, MA) [63]. Briefly, a recorded video was turned into a binary video, the noise and artifacts were removed to locate the object of interest in each frame, and the objects in successive frames were linked using the nearest-neighbor method. The tracking results enabled the measurement of critical motility parameters of each individual BacteriaBot such as average motion directionality [76] and chemotactic directionality. Herein, chemotactic directionality is defined as the

magnitude of the displacement vector projected on the x-axis (i.e. chemoattractant gradient direction) over the total distance traveled by the BacteriaBot along the x-axis, and is expressed as:

$$\text{Chemotactic directionality} = \frac{\vec{r}_{end,x} - \vec{r}_{start,x}}{\sum_{i=1}^{N} \Delta \vec{r}_{i,x}} \qquad (3\text{-}2)$$

where $\vec{r}_{start,x}$ and $\vec{r}_{end,x}$ are respectively the position vectors of the start point and the end point of the BacteriaBot trajectory, $\Delta \vec{r}_{i,x}$ is the distance travelled during the time step i, and N is the number of time steps.

3.3 Results and discussion

Chemical concentration gradients in the hydrogel device, described above, were characterized using fluorescein (MW 332 Da) as the model solute for L-aspartic acid (MW 133.1 Da) which is a known chemoattractant for *E. coli* K-12 [83] (see Fig. A.1). This chemoattractant was selected and used throughout this study because aspartate receptors have been suggested to play an essential role in directing therapeutic bacteria towards tumor cells [28]. The CPC values which reflect the bacterial distribution in the bacterial chemotaxis assay were calculated using Eqn. 3-1 for each concentration gradient and plotted in Fig. 3.3 (a). The strongest response among the four concentration gradients that we examined was observed at 1.7×10^{-5} M mm^{-1} whereas the 1.7×10^{-3} M mm^{-1} gradient elicited the weakest chemotactic response. These results are in agreement with previous chemotaxis studies where steeper gradients did not necessarily yield a stronger chemotactic response due to saturation of chemoreceptors at high chemoattractant concentrations [84]. A Negative control experiment with motility buffer flowed in both side channels was

performed to verify that the migration of bacteria towards one specific side is only because of chemotaxis. Representative images of bacterial distribution in the presence of these two chemoattractant gradients are shown in Fig. 3.3 (b).

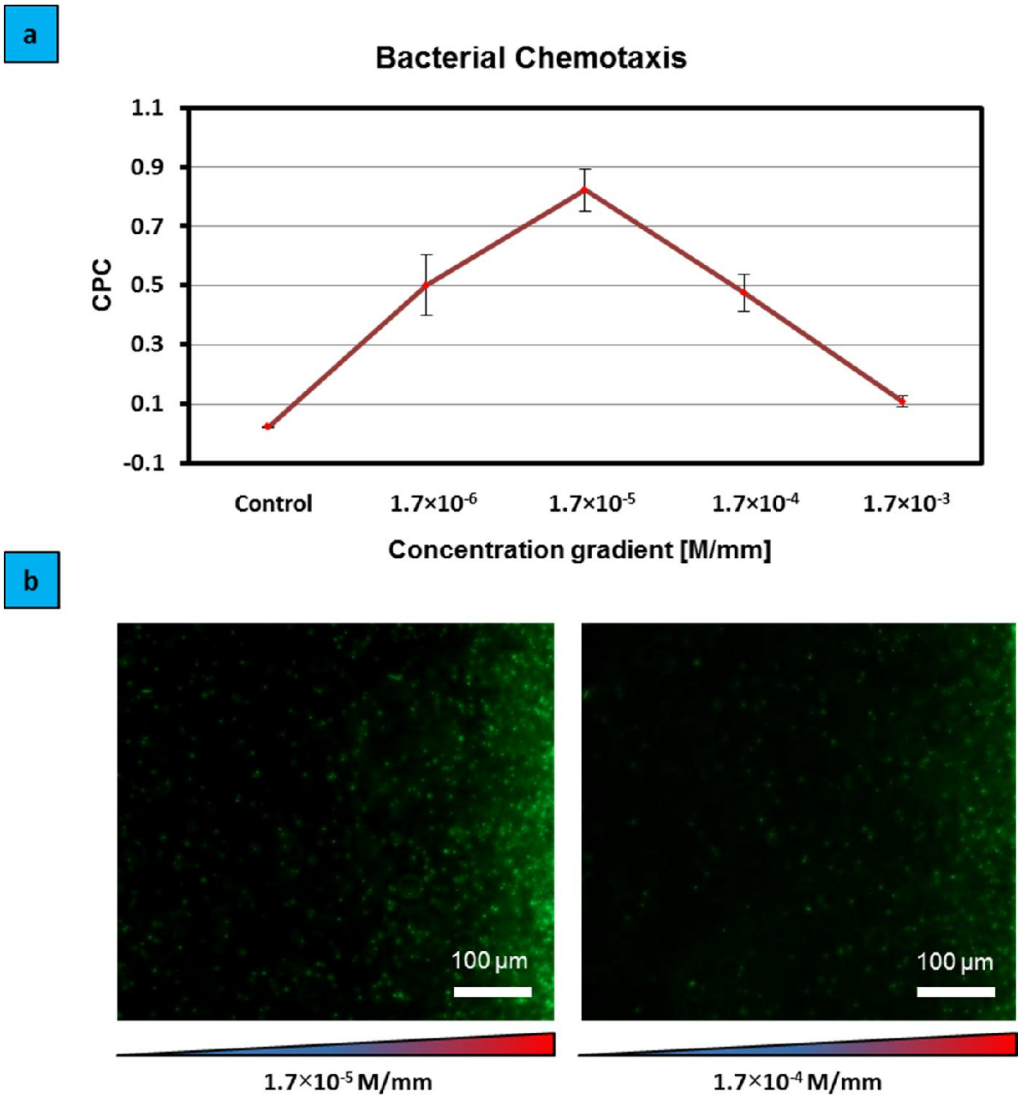

Figure 3.3 (a) Steady-state chemotaxis partition coefficient (CPC) values for *E. coli* MG1655m in response to different gradients of L-aspartic acid; (b) Steady-state bacterial distribution in the presence of 1.7×10^{-5} M mm^{-1} and 1.7×10^{-4} M mm^{-1} L-aspartic acid.

ED-shaped carboxylate polystyrene particles (5 μm× 11 μm× 2 μm, on average) were fabricated as described above. This particular shape was selected due to its longer half-life in blood circulation compared to spherical particles [12]. Spherical and ED-shaped BacteriaBots were constructed taking advantage of the high affinity between streptavidin and biotinylated anti-*E. coli* antibody. The anti-*E. coli* LPS antibody used here was raised against the "O" antigens present on the bacterial cell surface which resulted in the attachment of the antibody-decorated bacteria to the streptavidin-coated particles only through their cell bodies (and not their flagella). The strong non-covalent bond between biotin and streptavidin [85] ensured the stability of the complex between bacteria and microparticles in our experimental conditions. Co-localization of *E. coli* bacteria and polystyrene particles was verified by inspecting a 10 μl aliquot of the BacteriaBots suspension between two glass coverslips separated by grease using fluorescence microscopy. Representative scanning electron microscopy (SEM) images of the fabricated ED polystyrene particles and fluorescence images of spherical and ED-shaped BacteriaBots are depicted in Fig. 3.1 (c) and (d). The number of bacteria attached to either spherical or ED microparticles ranged from 8 to 15. We have previously shown that this level of variation in the number of randomly attached bacteria has minimal effect on the motile behavior of BacteriaBots [76].

To investigate the relative importance of chemical cues (i.e. chemoattractant gradient) and geometrical cues (i.e. body shape) on the motile behavior of BacteriaBots, spherical and ED-shaped BacteriaBots were loaded into the microfluidic device after establishing a 1.7×10^{-5} M mm^{-1} gradient of L-aspartic acid in the center channel of the device (along with a control experiment in the absence of the chemoattractant gradient). This concentration gradient was used as it was found to yield the highest CPC for *E. coli* MG1655m chemotaxis towards L-aspartic

acid (see Fig. 3.3 (a)). After the gradient was established, the migration profile of BacteriaBots was monitored every 5 min for the duration of the experiment. As shown in Fig. 3.4 (a), the CPC values for spherical and ED-shaped BacteriaBots respectively reached 0.78 ± 0.13 and 0.76 ± 0.14 after 15 min. No significant change in the CPC values was observed after 15 min. Statistical analysis demonstrates lack of significant difference between the chemotactic responses of EDs and spheres ($n=5$, $p>0.05$). Fig. 3.4 (b) depicts two snapshots of a mixed population of both shapes of BacteriaBots in the center channel at the beginning and end of the experiment. As expected, chemotactic BacteriaBots localized at the hydrogel wall nearest to the chemoattractant channel (i.e. at the highest concentration of chemoattractant). Complementary control experiments showed that bacteria-free particles are not able to reach the chemoattractant side (data not shown). In addition to CPC, which is a measure of the direction of BacteriaBot migration at population scale, motility parameters of individual BacteriaBots can be calculated to quantify the strength of the chemotactic response. To analyze the migration of individual BacteriaBots along the gradient, 10 min long videos were captured at 2 frames per second and chemotactic directionality of individual BacteriaBots was calculated using the custom image processing routine as described previously (see Eqn. (3-2)). The average chemotactic directionality values of chemotactic spherical and ED BacteriaBots were respectively 0.19 ± 0.13 and 0.23 ± 0.14 and were not statistically different ($P>0.05$). Thus, the strengths of the chemotactic migration of spherical and ED BacteriaBots were similar in the presence of L-aspartic acid gradient. This further corroborates the dominance of chemotactic response over body shape observed earlier in this study, because we had previously shown that BacteriaBots with elongated shapes move in a more directional manner compared to their spherical counterparts in an isotropic (i.e. non-chemotactic) environment [76]. The directionality values of

spherical and ED BacteriaBots in an isotropic environment were respectively 0.21 ± 0.12 and 0.28 ± 0.11. This indicates a higher directionality, however towards a random direction, for ED

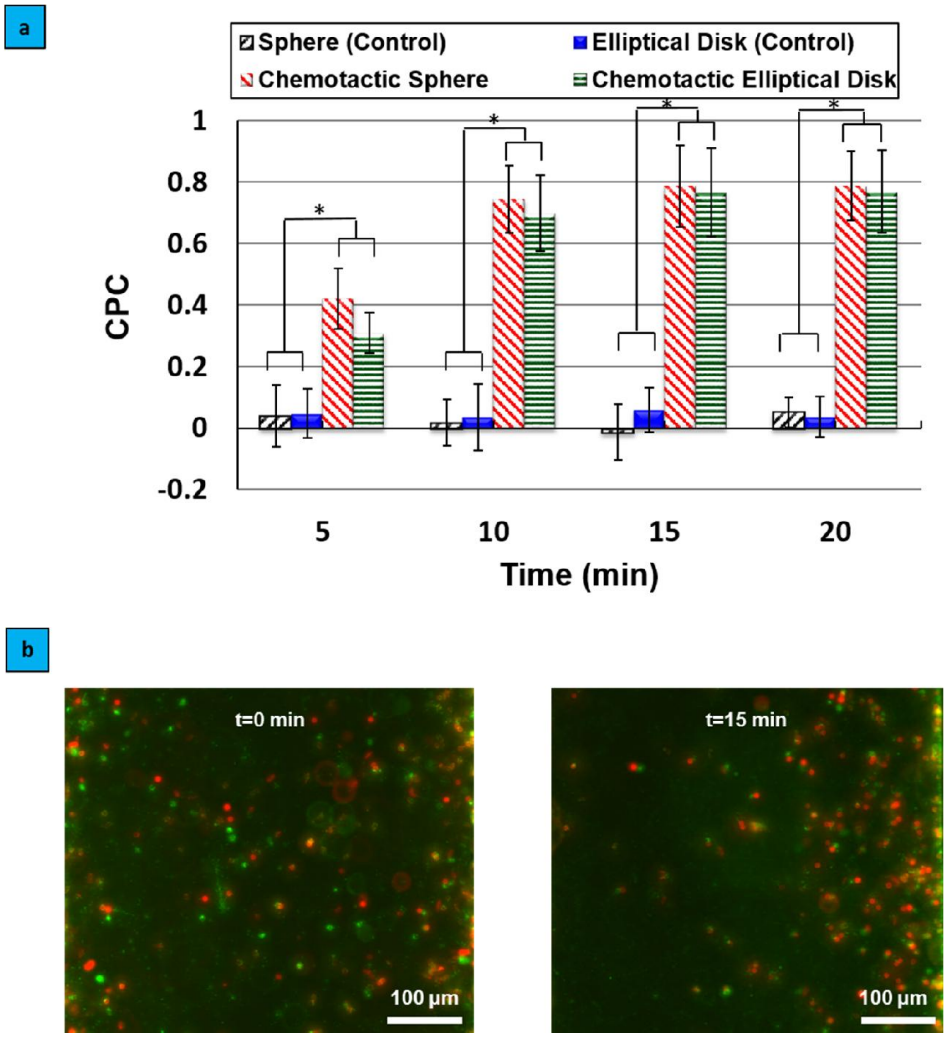

Figure 3.4 (a) Chemotaxis partition coefficient (CPC) values for spherical and elliptical disk-shaped BacteriaBots migrating in the absence (negative control) and presence of 1.7×10^{-5} M mm^{-1} L-aspartic acid; (b) Representative images of BacteriaBots at the beginning (t=0 min) of a chemotaxis experiment (left) and at steady state (right) when BacteriaBots accumulated in the region of highest L-aspartic acid concentration (t=15 min).

BacteriaBots compared to spherical ones in absence of chemoattractant gradients ($P \leq 0.05$). Polar plots of representative trajectories of BacteriaBots in the absence and presence of a chemical concentration gradient, shown in Fig. 3.5, illustrate that BacteriaBots moved in a biased fashion when they are subjected to a favorable chemical gradient.

The dominance of chemotaxis over body shape was further investigated in the presence of a steeper gradient of the chemoattractant (along with a control experiment in the absence of the chemoattractant gradient) to elucidate the effect of chemoattractant gradient slope on the motile behavior of BacteriaBots. BacteriaBots were subjected to a 1.7×10^{-4} M mm^{-1} gradient of L-aspartic acid which was shown to yield a weaker bacterial chemotactic response as compared to that due to the 1.7×10^{-5} M mm^{-1} gradient (Fig. 3.3 (a)).

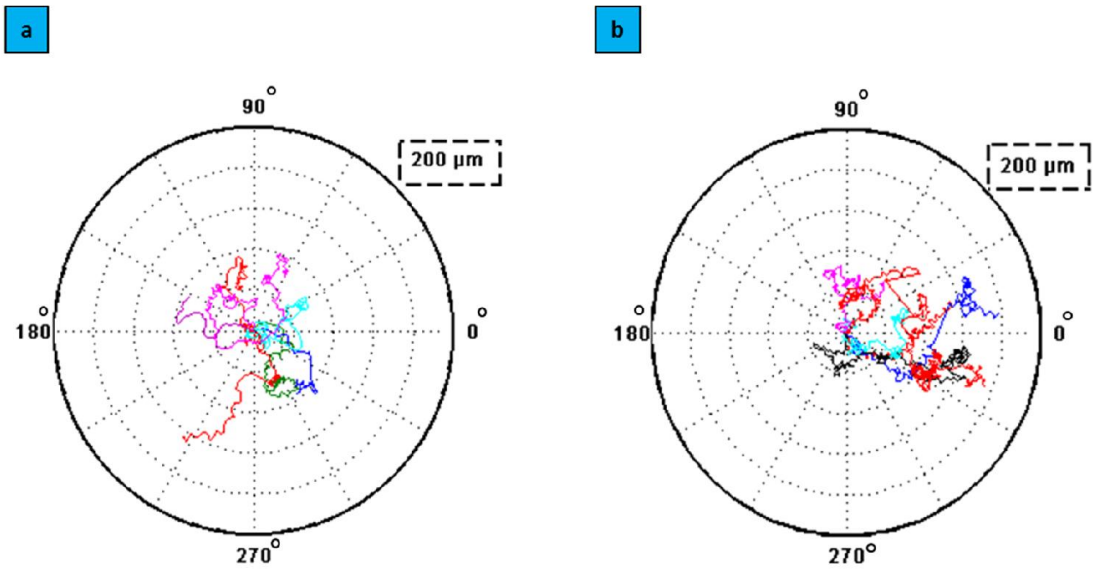

Figure 3.5 Representative trajectories of BacteriaBots migrating (a) in a non-chemotactic environment, and (b) in presence of 1.7×10^{-5} M mm^{-1} L-aspartic acid. Individual trajectories are represented in different colors. The biased trajectories indicate the effect of chemotaxis on the directionality of BacteriaBots' motion up the chemical gradient along the x-axis. The radius of both polar plots is 200 µm.

The migration profile of the BacteriaBots was recorded in the form of videos every 5 min and the chemotactic response was quantified by calculating CPC values, as depicted in Fig. 3.6. For this gradient, spherical and ED BacteriaBots respectively reached CPC values of 0.78 ± 0.06 and 0.75 ± 0.07 after 40 min which were not significantly different ($n=5$, $p>0.05$). No significant change in the CPC values was observed after 40 min. The insignificant difference between the CPC values of spherical and ED BacteriaBots, regardless of the slope of chemoattractant gradient, reaffirms the consistent dominance of chemotaxis over body shape in interstitial transport of BacteriaBots where bacteria are directed by chemical gradients.

In summary, ED-shaped BacteriaBots were developed to investigate the roles of chemical steering (chemotaxis) and body shape in transport behavior of bacteria-based drug delivery systems. A hydrogel-based microfluidic device was utilized to study the chemotaxis of spherical and ED-shaped BacteriaBots in presence of two different gradients of the chemoattractant, L-aspartic acid. Experimental results showed that chemotactic response dominates the effect of body shape and thus, the non-spherical BacteriaBots may be more favorable for drug delivery applications owing to the known benefits of using non-spherical particles for vascular transport. Moreover, this dominance was not disrupted by changing the chemical concentration gradient slope. The constructed autonomous non-spherical BacteriaBots under the control of chemotaxis hold great promise for nanomedicine and bio-nanorobotic applications owing to the tailored shape of the particles and targeting bacteria. Our future work will concentrate on using genetically modified bacteria which can navigate autonomously towards chemoattractant sources while carrying their non-spherical cargos, and accomplish pre-programmed functions upon arrival (e.g. cargo distribution) at desired sites.

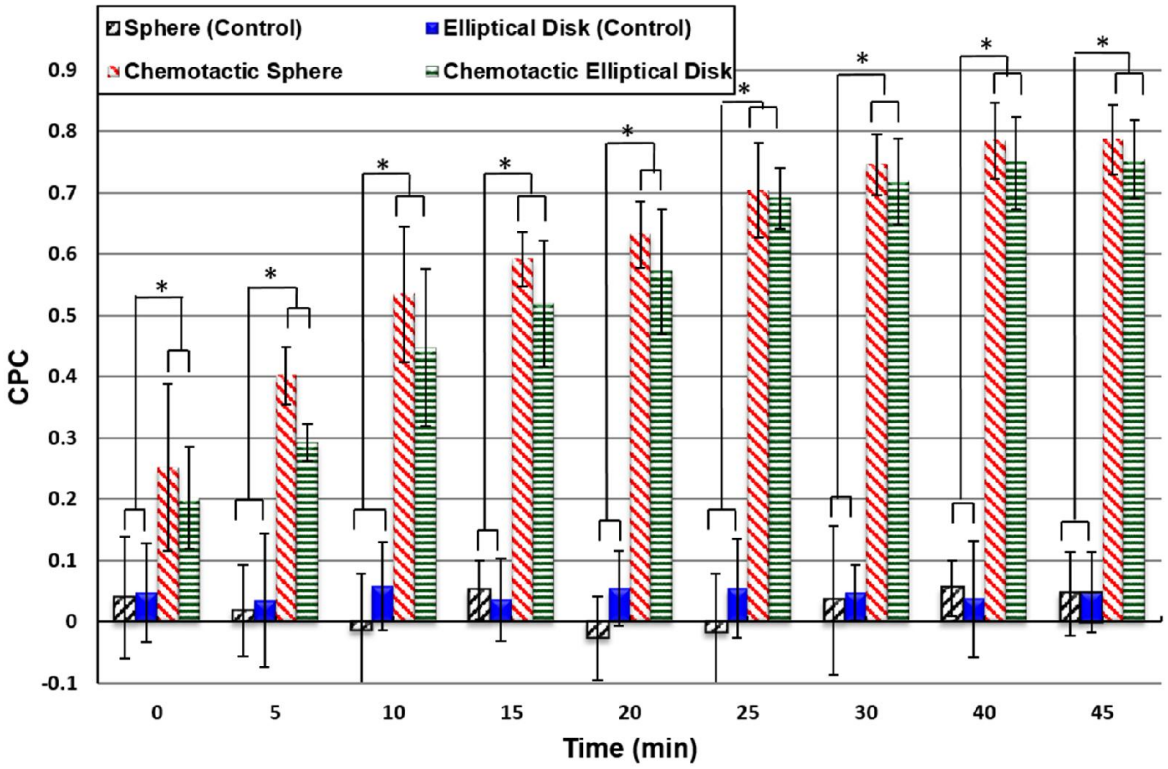

Figure 3.6 Chemotaxis partition coefficient (CPC) values for spherical and elliptical disk-shaped BacteriaBots migrating in the absence (negative control) and presence of 1.7×10^{-4} M mm^{-1} L-aspartic acid.

3.4 Conclusions

The autonomous BacteriaBots fabricated in this study are a new generation of bacteria-based cargo carriers expected to exhibit prolonged circulation in the bloodstream coupled with improved targeting and active interstitial transport, desirable for drug delivery purposes. BacteriaBots in two different shapes, sphere and elliptical disk, were steered by establishing chemoattractant concentration gradients within a hydrogel-based microfluidic device. The experimental results showed that spherical and elliptical disk-shaped BacteriaBots yield similar steady-state chemotactic responses if subjected to the chemoattractant, L-aspartic acid. These

results suggest that chemotactic response dominates body shape in interstitial transport; thus, the fabricated non-spherical BacteriaBots may be more favorable for drug delivery applications owing to the aforementioned transport characteristics of these flat and elongated carriers in bloodstream. We believe this lab-on-a-chip approach can be further developed to enable replicating biochemical and biophysical aspects of *in-vivo* microenvironments in which BacteriaBots are likely to encounter multiple gradients of chemoeffectors in interstitium and investigate interstitial transport characteristics of BacteriaBots in presence of precisely controlled gradients of such disease biomarkers.

Appendix A

A.1 Microfluidic device characterization and simulation

Chemical concentration gradients in the PEG-DA hydrogel microfluidic device was characterized using fluorescein (MW 332 Da, Sigma-Aldrich) as the model solute for L-aspartic acid, the chemoattractant used in this study. First, PBS solution was manually loaded in the center channel and the corresponding tube was clamped after filling up the channel to prevent any fluid flow and liquid evaporation. To establish a concentration gradient of fluorescein in the device, fluorescein/PBS and blank PBS buffer solutions were flowed in the two side feeder channels driven by a syringe pump (Harvard Apparatus, PHD 2000, South Natick, MA) at a flow rate of 5 μl min^{-1} so that fluorescein can diffuse laterally in the hydrogel walls and establish a quasi-steady linear gradient in the no-flow center channel. The fluorescence intensity across the device was imaged under a Zeiss AxioObserver Z1 inverted microscope equipped with a 2.5× objective, a GFP filter cube and an AxioCam HSm camera. The ImageJ software (NIH, Bethesda, MD) was used to analyze the experimentally acquired fluorescence intensity profiles and calibrate the gradient profile. A representative image of the three-channel hydrogel microfluidic device and the fluorescence profile across the width of the center channel are shown in Fig. A.1 (a) and (b). The time required to establish a steady concentration gradient of fluorescein in the device is governed by the diffusion coefficient of fluorescein in PEG-DA hydrogel and also by the width of hydrogel walls and channels.

The generation of chemical gradients in the three-channel microfluidic device was simulated in COMSOL® Multiphysics (Burlington, MA) to validate the slope of the experimentally observed linear concentration gradient of fluorescein. In this simulation, the diffusion coefficient of fluorescein in PBS was set as 2.7×10^{-6} cm^2 sec^{-1}. The diffusion coefficient of fluorescein in PEG-

DA hydrogel (MW 700 Da) was previously measured as 1.8×10^{-6} cm^2 sec^{-1} using Franz diffusion cell experiment [79]. A simulated gradient profile across the device is shown in Fig. A.1 (c). The fabricated device provided quasi-steady linear chemical concentration gradients for chemotaxis studies and simulation results show that the gradient reaches steady state after 35 min.

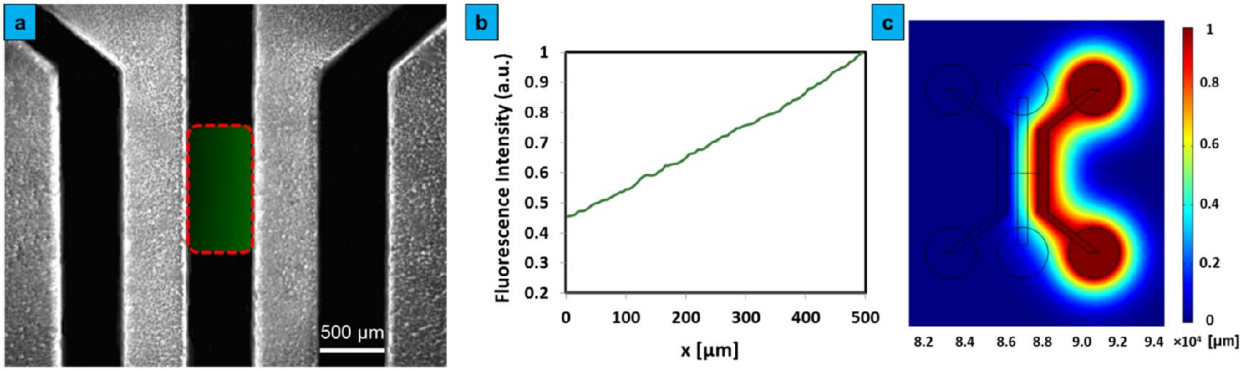

Figure A.1 (a) Three-channel hydrogel microfluidic device (top view) overlaid with the fluorescence gradient of fluorescein inside the selected rectangular region in the center channel; (b) Fluorescence profile across the width of the center channel; (c) COMSOL® simulations indicate that the steady-state chemical concentration gradient is reached after 35 min.

Chapter 4: Spatiotemporally High-Throughput Characterization of Bacterial/BacteriaBot Quorum-Sensing Response*

Abstract

Characterization of bacterial innate and engineered cooperative behavior, regulated through chemical signaling in a process known as quorum sensing, is critical to development of a myriad of bacteria-enabled systems including bio-hybrid drug delivery systems and bio-hybrid mobile sensor networks. Here, it is demonstrated, for the first time, that microfluidic diffusive mixers can be used for spatiotemporally high-throughput characterization of a bacterial quorum-sensing response. Using this batch characterization method, the quorum-sensing response in *Escherichia coli* MG1655, transformed with *luxR* from *Vibrio fischeri* and a GFP reporter ligated to the *lux* operon promoter, in the presence of 1-100 nM exogenous N-3-oxo-hexanoyl-L-homoserine lactone molecules has been quantified. This method provides a rapid and facile tool for high-throughput characterization of the quorum-sensing response of genetically modified bacteria in the presence of a wide concentration range of signaling molecules with a precision of ± 0.5 nM. Furthermore, the quorum-sensing response of BacteriaBots has been characterized to determine if the results obtained from a large bacterial population can serve as a robust predictive tool for the small bacterial population attached to each BacteriaBot.

*This chapter is under review in the form of a journal article: A. Sahari, M. A. Traore, A. M. Stevens, B. E. Scharf, and B. Behkam, "Towards development of an autonomous network of bacteria-based delivery systems (BacteriaBots): Spatiotemporally High-Throughput Characterization of Bacterial Quorum-Sensing Response". Analytical Chemistry, 2014.
M. A. Traore contributed to this work with his help with the design and simulation of the microfluidic diffusive mixer. A. M. Stevens constructed the quorum sensing plasmids and contributed to the analysis of the results. B. E. Scharf contributed to the bacterial transformation. B. Behkam directed this effort and contributed to the experiment design, analysis of the results and manuscript preparation.

Many bacterial species produce, release and respond to signaling molecules, called autoinducers, in order to effectively communicate information with each other and/or monitor the mass transport properties of their immediate environment through a process termed quorum sensing (QS) [39, 86]. Each autoinducer structure can be recognized by the same or sometimes other bacterial species and trigger expression of target genes, if a critical concentration of the autoinducer is reached. This signal transduction enables the bacteria to coordinate their group activities such as light production, pathogenesis and virulence, swarming motility and biofilm formation [45-49]. The cooperative behavior of bacteria can be exploited for generating a mobile network of bio-hybrid systems such as the bacteria-based drug delivery systems (BacteriaBots) that have been recently developed [5, 63, 76]. Each BacteriaBot is comprised of live disease-targeting bacteria harboring QS-based genetic circuits coupled with micro/nanoscale polymeric particles. A BacteriaBot is a simple bio-hybrid system with limited individual capabilities; thus BacteriaBots are envisioned to execute cooperative theranostic tasks at targeted disease sites by harnessing BacteriaBot-BacteriaBot communication. Characterization of the QS-regulated response of bacteria is critical to development of such systems.

Engineered bacteria containing QS-based genetic circuits have been used as bioreporters for quantifying autoinducer concentrations [87]. Although using such bioreporters leads to characterization of QS response with a higher sensitivity compared to conventional analytical methods [88], a high-throughput platform that can rapidly characterize the QS behavior of a bioreporter in response to a wide range of autoinducer concentrations is still missing. Recognizing the role of diffusive properties of autoinducers, in addition to that of bacterial population number on QS response [86, 89], microfluidic platforms have been utilized for studying the effect of chemical signaling on bacterial growth and biofilm formation [90, 91] as

well as for inducing a desired QS response from individual (or from a low population density of) bacteria [92-94]. However, there is no reported microfluidic assay for investigating the effect of a wide range of autoinducer concentrations on the QS-based behavior of a bioreporter. In this work, a spatiotemporally high-throughput characterization of the bacterial QS response of a model bioreporter to a wide range of exogenous acyl-homoserine lactone (AHL) autoinducer concentrations in a single experiment is reported utilizing a microfluidic diffusive mixer platform. The advantage of this high-throughput method compared to its commonly used counterpart (i.e. well-plate assays) is in capturing the time-dependency in response while maintaining a constant concentration of the exogenous AHL. Such experimental characterization of bacterial QS also contributes to understanding the effective "calling distance" [95] over which BacteriaBots can communicate with each other and to designing and predicting the collaborative behavior of a population of BacteriaBots [96]. Furthermore, this characterization platform will be beneficial to the development of QS-based biosensing systems that have been suggested for diagnosis of bacteria-related diseases [97].

AHL-mediated systems, which are present in many Gram-negative proteobacteria, are the simplest QS paradigm [43]. Specifically, the canonical LuxIR family falls in the category of AHL-based communication systems in which AHL is produced by LuxI autoinducer synthase and released in the extracellular environment. At a critical AHL concentration, the autoinducer molecule binds specifically to the LuxR regulatory protein and this complex regulates downstream genes upon binding to the *lux* box region [39]. The typical example of Gram-negative proteobacteria containing a LuxIR network is the marine bacterium, *Vibrio fischeri*, which has all the genes required for monitoring its population density and activating expression of luminescence genes through production of the autoinducer, N-(3-oxo-hexanoyl)-L-

homoserine lactone (3-oxo-C6-HSL) [50]. Synthetic biology has provided the tools for modulating existing biological networks and/or constructing recombinant plasmids to enable the host cells to perform novel tasks such as QS in addition to their innate cellular processes [53, 54]. For example, the transfer of the whole or a part of the LuxIR genetic system from *V. fischeri* to *Escherichia coli* has programmed the transformed bacteria to acquire QS-induced programmed population control via regulated killing of cells [58], and invasion of cancer cells [60]. In this study, non-motile, non-flagellated *E. coli* MG1655 Δ*motAB* Δ*fliC* [98] were transformed with the AHL-responsive segment of the LuxIR network from *V. fischeri* through inserting the pLVA01 plasmid construct (Ap^r; pUC18Not-*luxR*-P_{luxI}-RBSII-*gfp*(LVA)-T_0-T_1) [91] into the bacteria using standard protocols [81]. This engineered *E. coli* MG1655 expresses the LuxR regulator but lacks the ability to synthesize AHL. However, when a critical concentration of AHL is provided exogenously, the pLVA01 plasmid expresses green fluorescent protein (GFP) under the control of the *lux* operon promoter. The QS signaling pathway in the receiver-only (*luxI*$^-$) *E. coli* MG1655, hereafter referred to as *E. coli* MG1655R, and the structure of the AHL signal are shown in Fig. 4.1 (a). Herein, the characterization of the QS response of the bioreporter, *E. coli* MG1655R containing the GFP-expressing pLVA01 plasmid, was facilitated through a rapid screening of a wide range of AHL concentrations in a microfluidic diffusive mixer that has been extensively used for cell chemotaxis studies [99].

The microfluidic device was fabricated in PDMS [99] using conventional soft lithography methods [100] to establish nearly linear concentration gradients of the autoinducer molecules for a uniform layer of bacteria, which enabled characterization of the bacterial QS response to 1-100 nM of exogenous AHL concentrations in a single experiment. This microfluidic device consists of a gradient forming region and an observation channel where the surface-bound bacteria are

located (see Appendix B for the details of fabrication). The layout of the device is depicted in Fig. 4.1 (b). The branched network of microfluidic channels generates spatially controlled gradients of the autoinducer across the width of the channel and perpendicular to the fluid flow. A 400 µM fluorescein solution in DI water was used to characterize the device. Fluorescence intensity profiles were used to determine the concentration of fluorescein (model solute for AHL) at any position across or along the observation channel (see Appendix B for details). A representative fluorescence microscopy image of the chemical gradient across the width of the observation channel is shown in Fig. 4.1 (b).

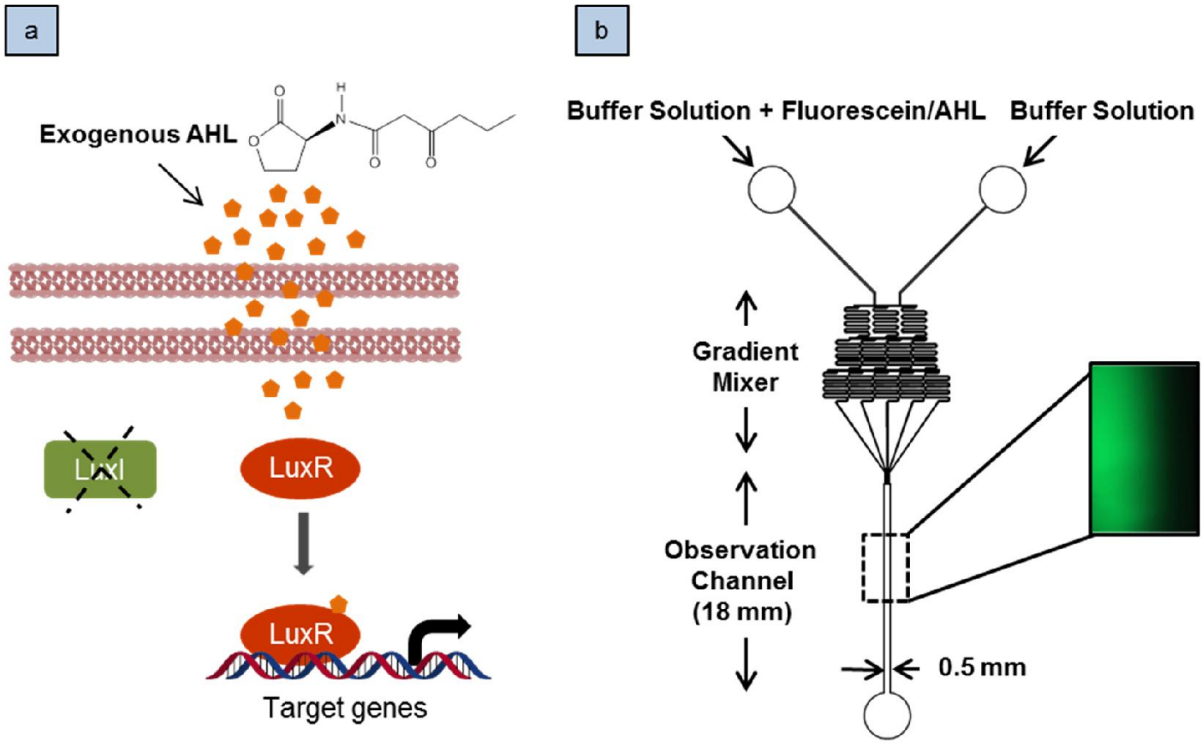

Figure 4.1 (a) The LuxIR QS network deficient in AHL signal synthesis; (b) The layout of the PDMS microfluidic device layer and a representative gradient of fluorescein across the width of the observation channel.

The non-motile receiver-only *E. coli* MG1655R bacteria, generated as described above, were grown overnight at 30 ˚C and 150 rpm shaking in 10 ml of Luria-Bertani broth (LB broth; 1% tryptone, 0.5% yeast and 0.5% NaCl) supplemented with ampicillin (100 μg ml^{-1}) and then diluted 1:100 in LB medium to start a 10 ml of fresh bacterial culture . The assembled microfluidic device was sterilized under UV light for 20 min prior to the experiment. After washing the device with sterile 1× phosphate buffered saline solution, the main channel was incubated for two hours with a 0.005% (w/v) poly-$_L$-lysine in DI water. When the bacterial culture reached an OD_{600} of 0.5, 1 ml of the culture was harvested by centrifugation at 1,700 × g for 5 min and the resultant pellet was resuspended in 250 μl of RM medium (1 × M9 salts, 2% casamino acids, and 0.4% glucose) [101]. DI water was flowed into the device to wash out unbound poly-$_L$-lysine and then the non-motile cells were introduced into the device from the outlet. The outlet was blocked afterwards to allow for sedimentation of bacteria onto the surface. Use of the non-motile strain of *E. coli* MG1655 bacteria facilitated rapid formation of a bacterial layer on the bed of the main channel and also prevented previously shown disruption of the chemical gradients by flagellar mixing [102]. After 15 min, unbound bacteria were rinsed off and a 100 nM solution of 3-oxo-C6-homoserine lactone (N-(β-ketocaproyl)-L-homoserine lactone, Cayman Chemical) in RM medium (diluted from a 10 mM stock stored in DMSO) was flowed from one of the inlets and plain RM medium was flowed from the other inlet driven by a syringe pump (Harvard Apparatus, PHD 2000) at a 90 μl hr^{-1} flow rate to generate a nearly linear gradient of AHL (perpendicular to the direction of the flow) for the surface-bound bacteria. A close to linear AHL gradient was maintained throughout the observation channel for the entire duration of an experiment. All experiments were conducted at 30 ˚C using a Zeiss Axio-observer Z1 inverted fluorescence microscope equipped with a climate control incubation chamber.

Fluorescence images of the bacterial layer were acquired every 30 min for a total of 9 hours using a 10× objective lens. The exposure time of fluorescent images was 200 ms. Representative images of the QS-directed fluorescent response of the bacterial layer attached on the bed of the microfluidic device, 600 μm downstream in the observation channel, are shown in Fig. 4.2 (a). At least two independent experiments were conducted and images were acquired from two successive sections (each 890 μm in length) of the observation channel. To quantify the bacterial QS response, the observation channel was divided into 100 parallel sub-channels and the average fluorescence intensity value for the bacteria in each partition was calculated using ImageJ and MATLAB routines. The resultant dose-time-response curves (with ± 0.5 nM precision) are shown as a 3D plot in Fig. 4.2 (b) where the quantified bacterial QS response is presented using the log of the average fluorescence intensity as a function of AHL concentration and time. The average fluorescence intensity of bacteria increases with an increase in AHL concentration from 6 nM to 95 nM (the bacterial response near the PDMS walls was not quantified due to the existing artifacts). Using this dose-time-response plot, the bacterial QS response at any given time and concentration can be reported. Representative relative fluorescence intensity at 10 nM, 30 nM and 90 nM concentrations of AHL over the entire experiment are plotted separately and shown in Fig. 4.2 (c). The fluorescent response of the receiver bacteria resembles a first-order linear dynamic response and can be described by $\mathrm{y(t)} = K(\mathrm{c})\left(1 - e^{-t/\tau(c)}\right)$, where the time constant, $\tau(c)$, and the steady-state response of the system, $K(\mathrm{c})$, are both functions of the AHL concentration (see Appendix B for details). Exponential functions for characteristic response of the bacteria at 10 nM, 30 nM, and 90 nM concentrations of AHL are demonstrated in Fig. 4.2 (c). Characterizing the response of *E. coli* bacteria containing a QS-controlled GFP-expressing genetic circuit enables us to predict the coordinated behavior of a mobile network of

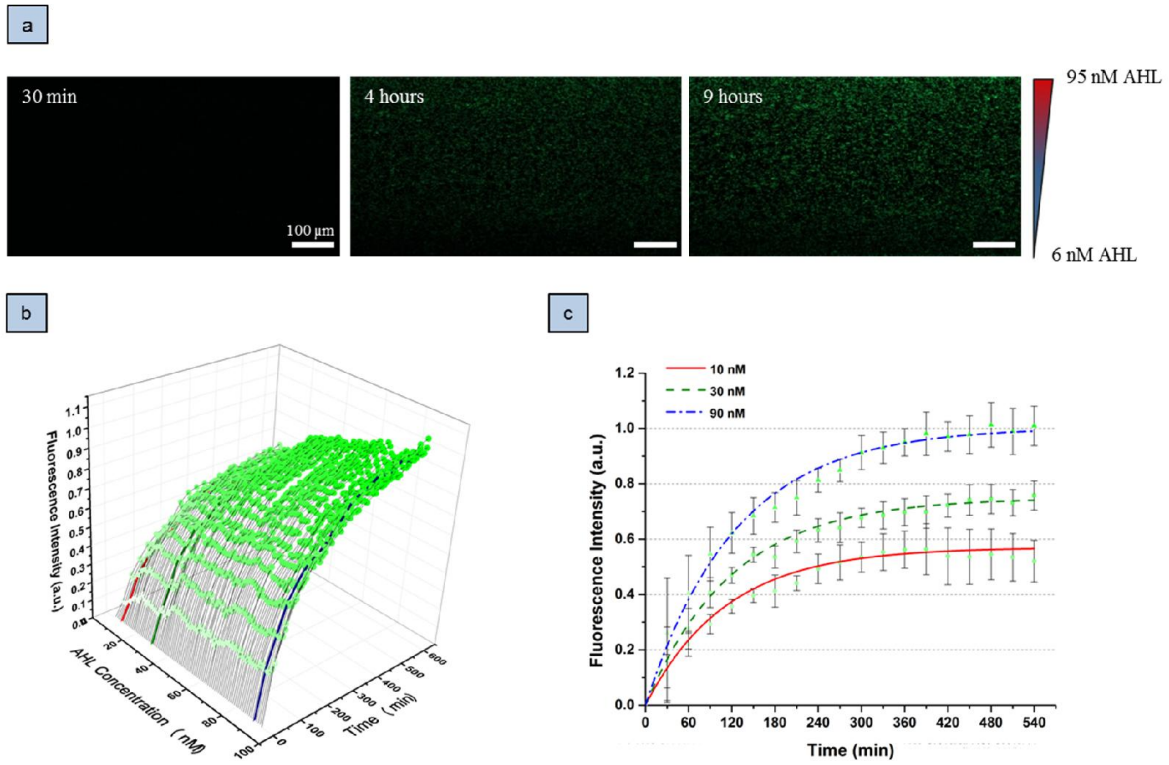

Figure 4.2 (a) Representative images of the quorum-sensing response of the bacterial layer attached to the bed of the microfluidic device at different time points; (b) Dose-time-response curves of the bacteria; (c) Representative fitted exponential curves for the quantified fluorescence response of the bacteria at 10 ± 0.5 nM (red), 30 ± 0.5 nM (green) and 90 ± 0.5 nM (blue) concentrations of AHL. The error bars represent standard deviation.

BacteriaBots with the engineered bacteria as the biotic constituent of the system [96].

To ensure that results obtained from a large bacterial population can serve as a robust predictive tool for the small bacterial population on each BacteriaBot, the QS response of BacteriaBots was characterized next. To construct the BacteriaBots, flat elliptical disk-shaped (ED) particles were conjugated with *E. coli* MG1655R bacteria taking advantage of the strong streptavidin-biotin bond. The ED particles were fabricated from 6 µm diameter carboxylate polystyrene

microspheres using a high-throughput particle casting and mechanical stretching technique. This body geometry of BacteriaBots was selected to have all of the attached bacteria in focus and facilitate the acquisition of fluorescence images. The number of bacteria attached on the particles varied between 4 and 8. BacteriaBots were introduced into a microfluidic device coated with poly-$_L$-lysine and a QS response characterization experiment was conducted as described above for bacteria. Fluorescence images were acquired every 1 hour for 4 hours this time using a 40× objective lens to distinguish the bacteria attached on the particles. The exposure time of green fluorescence imaging was 200 msec. The average fluorescence intensity of the small population of bacteria attached to the elliptical disk-shaped particles located at the middle point of the observation channel (50 ± 1 nM) was calculated after subtracting the background and compared with that of the bacteria directly attached on the bed of the microfluidic device (see Fig. 4.3 (a)). One-way ANOVA and Tukey's test was used for comparing the mean fluorescence values, and report no statistically significant difference between the average response of the small population of bacteria on the BacteriaBots and large population of bacteria on the bed of the device (p>0.05). This further corroborates that characterizing the QS behavior of bacteria using the proposed microfluidic-based approach not only provides batch screening of the response to a wide range of AHL concentrations, but can also help to predict the behavior of individual BacteriaBots within a population. Representative recorded images of BacteriaBot QS are shown in Fig. 4.3 (b).

In conclusion, a high-throughput microfluidic-based approach has been demonstrated for batch quantification of the QS response of *E. coli* MG1655 transformed with *luxR* and a GFP reporter fused to the *lux* operon promoter from *V. fischeri* in the presence of a wide range of concentrations (1-100 nM) of 3-oxo-C6-homoserine lactone molecules at a precision of ±0.5 nM.

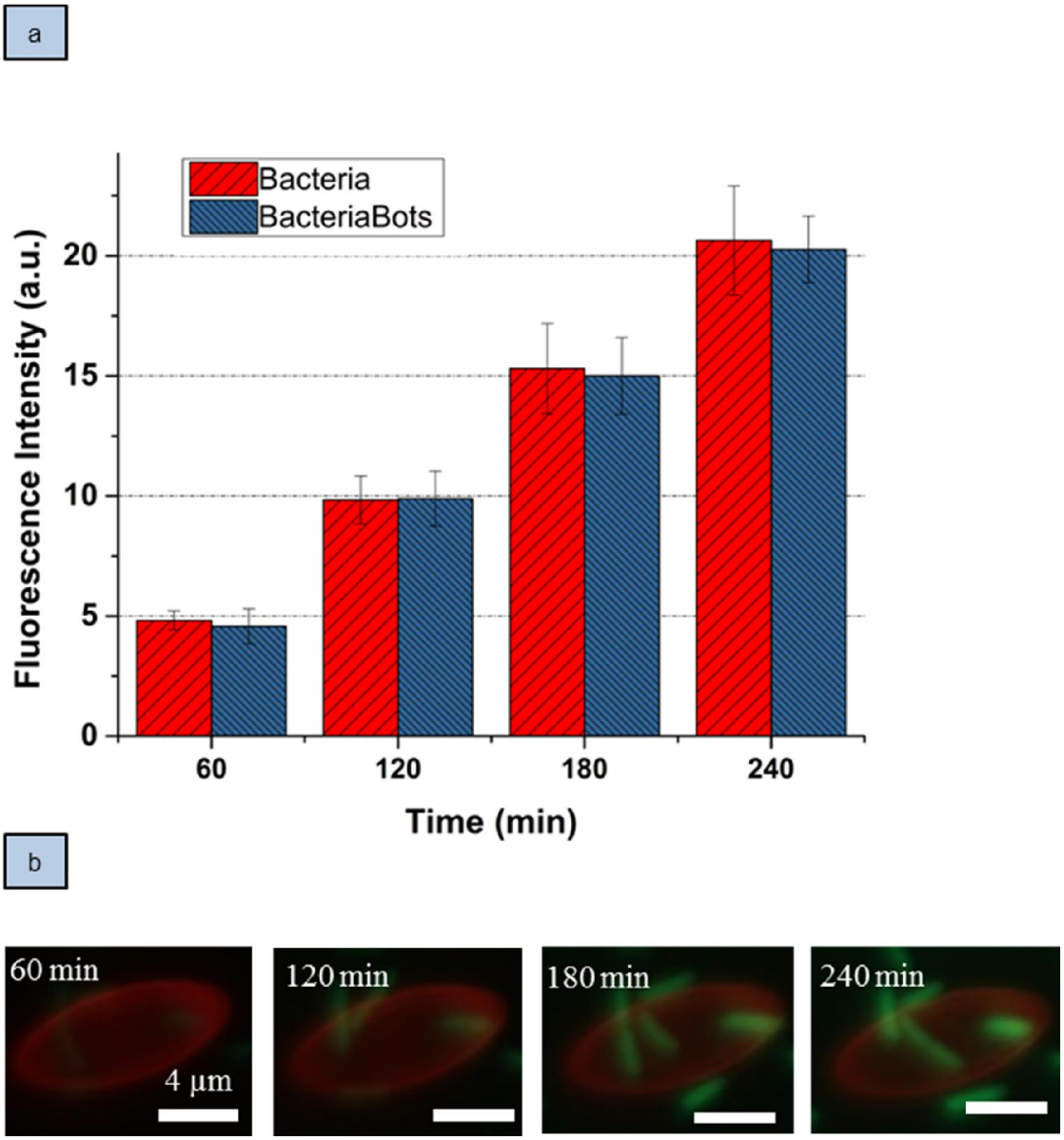

Figure 4.3 (a) Time-response of the particle-free bacteria and BacteriaBot-associated bacteria (n=9) located at the centerline of the microfluidic device where the concentration of AHL molecules is 50 ± 1 nM; (b) Representative fluorescence images of BacteriaBot quorum-sensing regulated GFP expression. The signal strength increases with time.

This characterization lays the foundation for predicting the collaborative behavior of a mobile network of BacteriaBots when the bacteria are pre-programmed with QS-based genetic circuits. These BacteriaBots can participate in coordinated group activities to accomplish autonomously directed tasks at the target site. The approach used in this study will find use for characterizing the QS response of a wide variety of bacterial species containing synthetic circuits that induce expression of fluorescent proteins.

Appendix B

Abstract

The microfluidic device was fabricated in PDMS using conventional soft lithography methods to establish nearly linear concentration gradients of the autoinducer molecules for a uniform layer of surface-bound bacteria. The branched network of microfluidic channels generates spatially controlled gradients of the autoinducer across the width of the channel and perpendicular to the fluid flow. A fluorescein solution was used to characterize the device. Furthermore, the dynamic QS response of *E. coli* MG1655 harboring the pLVA01 plasmid was modeled as a first-order linear dynamic system and the relevant coefficients were obtained from the experimental data for the QS-regulated fluorescence response of bacteria.

B.1 Microfluidic device fabrication and characterization

B.1.1 Microfluidic device fabrication

To achieve a 100 μm thick microfluidic device layer, a clean silicon wafer was spin-coated with SU-8 2050 negative photoresist (MicroChem Crop) at 500 rpm for 10 sec followed by a second spinning at 1,700 rpm for 1 min. The spin-coated wafer was soft-baked at 65 °C for 5 min followed by a 15 min hard bake at 95 °C. The baked wafer was then exposed to UV light (365 mW cm^{-1}, 50 sec) to transfer the pattern of a negative photolithography mask onto the wafer. Subsequently, the post-exposure bake was completed at 65 °C for 5 min followed by 10 min at 95 °C. Lastly, the wafer was developed by submerging it in SU-8 developer while shaking gently for 10 min. The fabricated master mold was then rinsed with isopropyl alcohol (IPA) and deionized (DI) water and coated with trichloro(1H,1H,2H,2H-perfluorooctyl) silane (Sigma-Aldrich) using a vacuum desiccator. PDMS was poured on the silicon wafer master mold,

degassed under vacuum, and cured at 75 °C for two hours. The PDMS layer was peeled off from the master and trimmed. The inlet and outlet ports were punched and the PDMS device layer was put in a plasma cleaner (Harrick Plasma, 200 mTorr, 18 W, 30 sec) (with the channel side facing up) along with a clean glass slide to activate both surfaces and accommodate for a strong bond. The device was assembled by pressing the two oxygen plasma-treated components together. The layout of the PDMS layer of the microfluidic device is depicted in Fig. B.1 (a).

B.1.2 Calibration of the chemical gradient profile

Chemical concentration gradient in the PDMS microfluidic device was characterized using fluorescein (MW 332 Da, Sigma-Aldrich) as the model solute for the quorum-sensing regulatory molecules (i.e. 3-oxo-C6-HSL, MW=213.2 Da). To establish a time-invariant concentration gradient of fluorescein across the width of the observation channel of the microfluidic device, a 400 μM solution of fluorescein in deionized (DI) water and blank DI water were loaded into the two inlet channels of the device using a syringe pump (Harvard Apparatus, PhD 2000) at a flow rate of 90 μl hr^{-1}. The resultant flow in the observation channel was 180 μl hr^{-1}. The fluorescence intensity across the observation channel was imaged under a Zeiss AxioObserver Z1 inverted microscope equipped with a 2.5× objective, a GFP filter cube, and an AxioCam MRm camera. ImageJ software (NIH, Bethesda, MD) was used to analyze the experimentally acquired fluorescence intensity profiles and calibrate the gradient profile. A representative fluorescence microscopy image and the associated intensity profile across the width of the observation channel are shown in Fig. B.1 (a) and (b). Also, a photograph of the microfluidic device is shown in Fig. B.1 (c).

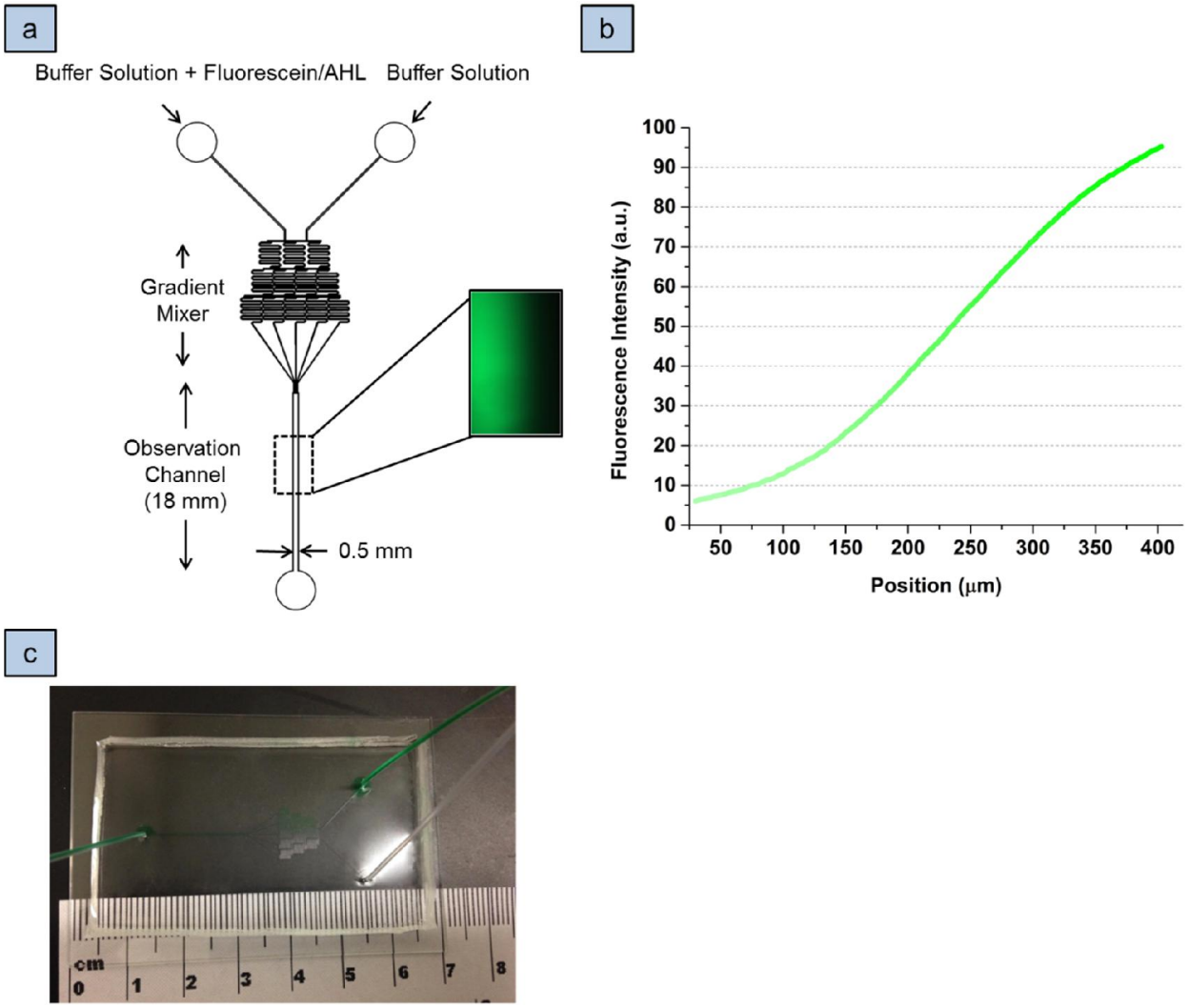

Figure B.1 (a) The layout of the PDMS microfluidic device layer; (b) Fluorescence profile across the width of the observation channel, 500 μm downstream from the channel entrance; (c) A photograph of the microfluidic device.

B.1.3 Modeling of the dynamic QS response

The dynamic QS response of *E. coli* MG1655 harboring the pLVA01 plasmid can be described as a first-order linear dynamic system. The differential equation describing the dynamics of the fluorescence response can be written in the standard input/output differential equation form as $\tau(c)\frac{dy}{dt}+\mathrm{y(t)}=K(c)$, where $\tau(c)$ the time constant and $K(\mathrm{c})$ the forcing function both depend on AHL concentration. The characteristic response to a step increase in the input level at 0 min is $\mathrm{y(t)}=K(\mathrm{c})\left(1-e^{-t/\tau(c)}\right)$. $\mathrm{K(c)}$ represents the steady-state value of the QS response of the bacteria and $\tau(c)$ is the time that it takes for the response to reach the 63% of its maximum. According to our experimental results, in the range of 1-100 nM AHL concentration, these two values depend on the AHL concentration (see Fig. B.2).

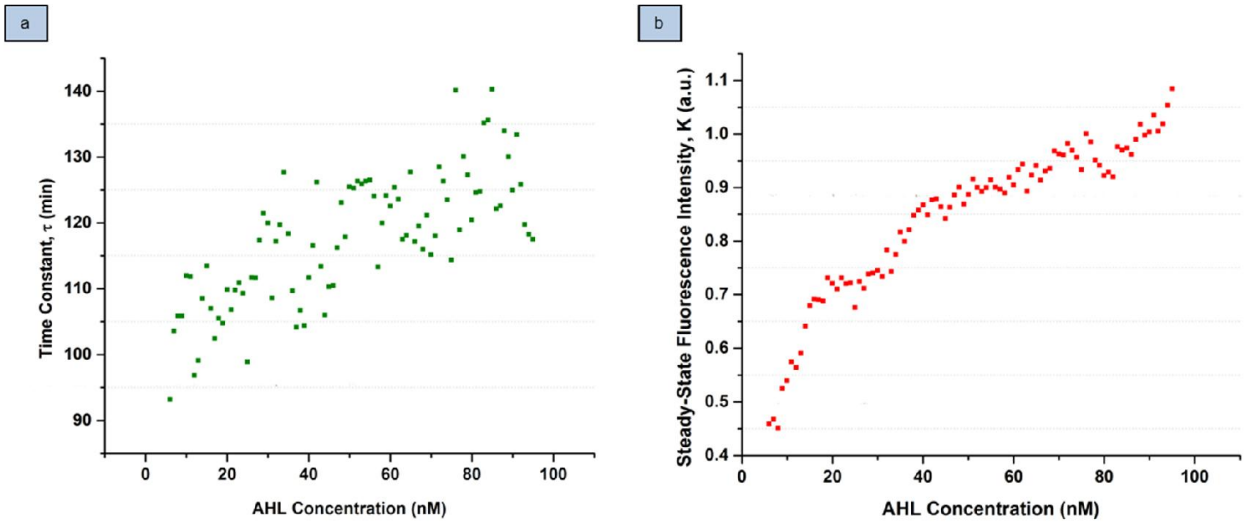

Figure B.2 (a) Time constant of the fluorescence response of the bacteria for the 6-95 nM concentration range of autoinducers; (b) the steady state values of the bacterial fluorescence response in the presence of different concentrations of autoinducers.

B.2 Systems biology modeling

Mathematical models can shed light on the principles of operation of a QS network and reveal its possible modes of behavior, which helps design more meaningful experiments towards understanding the functions associated with individual elements of the network. A simplified layout of the structural organization of a minimal LuxIR quorum-sensing network has been illustrated in Fig. B.3. In this system, the synthesized (or exogenously added) molecules of the autoinducer, 3-oxo-C6-HSL, diffuse through the cell wall, bind to the LuxR regulatory protein, and create the complex P which is usually transcriptionally competent in a dimeric form D. The formed transcription factor (P/D) directly activates transcription of the operon containing the LuxI synthase and other operons coding for the phenotype-specific genes.

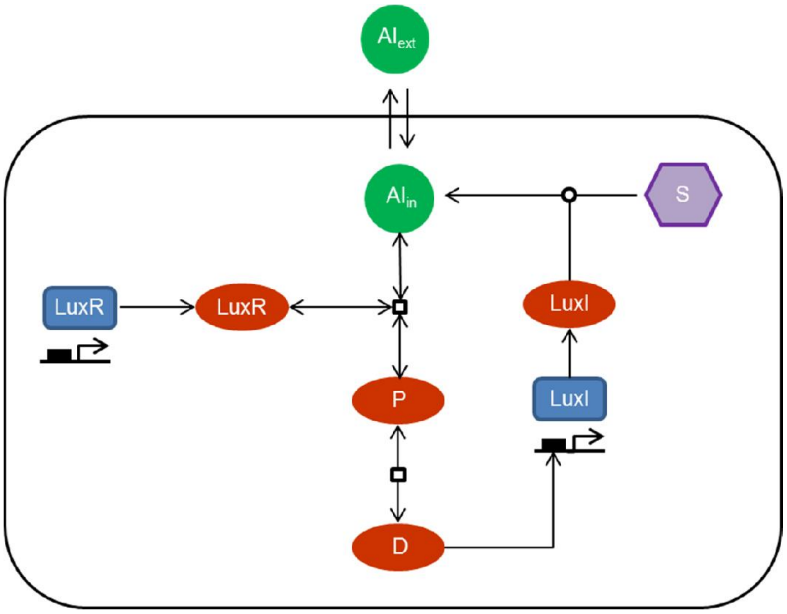

Figure B.3 A generic layout of the minimal LuxIR quorum-sensing network. Proteins and mRNA species are depicted as ellipses and rectangles respectively. P and D denote the complex of the LuxR protein and the autoinducer and the dimer of this complex. AI_{in} and AI_{ext} represent intracellular and extracellular concentrations of the autoinducer.

Here, a standard chemical kinetic approach was used based on general mass-action equations to describe temporal dynamics of the intracellular circuitry of the QS network while the extracellular concentration of AHL is maintained. The ordinary differential equations (ODEs) describing how concentrations of the involved proteins, RNA species, and AI change in time in the reduced minimal QS network [103] were adapted for the receiver-only bacteria (lacking LuxI synthase, see Fig. B.4) and are as follows:

$$\frac{dr}{dt} = k_1 - k_2 r \tag{B-1}$$

$$\frac{dR}{dt} = k_6 r - k_7 R - k_8 R.AI_{in} + k_{-8} P \tag{B-2}$$

$$\frac{dP}{dt} = k_8 R.AI_{in} - k_{-8} P - 2k_{13} P^2 + 2k_{-13} D \tag{B-3}$$

$$\frac{dD}{dt} = k_{13} P^2 + k_{-13} D \tag{B-4}$$

$$\frac{dAI_{in}}{dt} = -k_8 R.AI_{in} + k_{-8} P + k_D (AI_{ext} - AI_{in}) \tag{B-5}$$

where r, R, i respectively represent the concentration of the *luxR* mRNA, LuxR protein, luxI mRNA. Also, the link between the dynamics of the intracellular decision network and the observable phenotypic behavior (i.e. GFP expression) can be described as follows [104]:

$$\frac{dGFP_i}{dt} = k_{tr} P - k_{Gm} GFP_i - k_{Gd} GFP_i \tag{B-6}$$

$$\frac{dGFP_m}{dt} = k_{Gm} GFP_i - k_{Gd} GFP_m \tag{B-7}$$

where GFP_i and GFP_m respectively represent the concentration of the immature (inactive, non-fluorescent) GFP and mature (fully fluorescent) GFP.

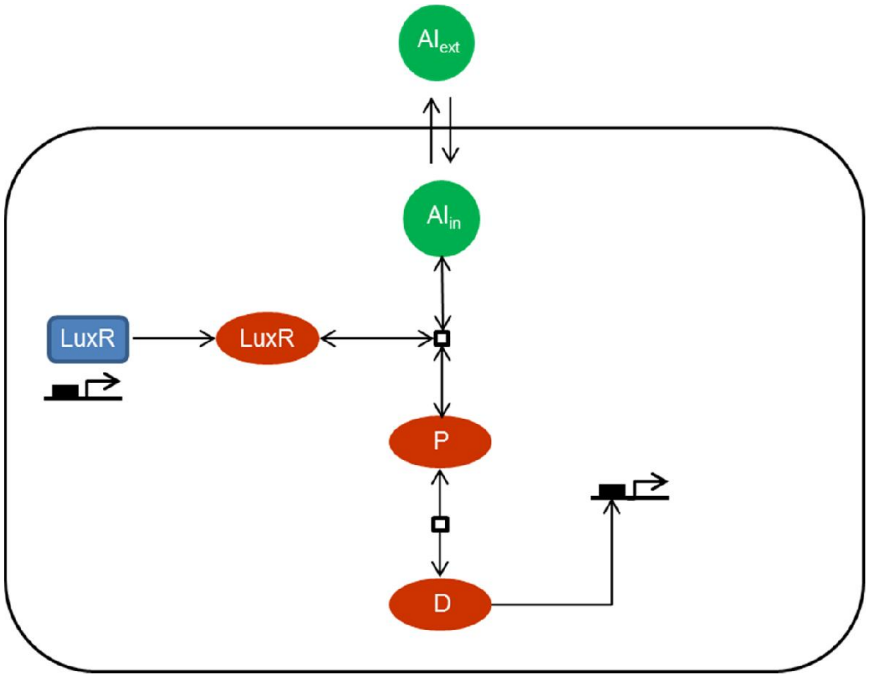

Figure B.4 The layout of a reduced minimal LuxIR quorum-sensing network for the receiver-only bacteria (*luxI*⁻ mutant).

The kinetic parameters are given in Table B.1 and the deterministic simulations were performed using MATLAB. The simulation results for 30 nM and 90 nM concentrations of AHL are shown in Fig. B.5 (1 molecule per cell corresponds to approximately 3 nM) [104]. As illustrated in Fig. B.5 (d), as the concentration of AHL increases, the time that it takes for the GFP response to reach its steady state decreases.

Table B.1 Rate constants for the metabolic processes of AHL-mediated GFP expression in the LuxI-LuxR genetic circuitry.

Rate Constant	Rate Description	Value	References
k_1	Transcription of *luxR*	1.5×10^{-2} m s^{-1}	[105] and [106]
k_2	Degradation of *luxR* mRNA	6.0×10^{-3} s^{-1}	[107]
k_6	Translation of *luxR* mRNA	1.6×10^{-2} s^{-1}	[106] and [108]
k_7	Degradation of LuxR protein	10^{-4} s^{-1}	[109]
k_8	Association of AHL and LuxR molecules	10^{-5} m^{-1} s^{-1}	[104]
k_{-8}	Dissociation of P	3.33×10^{-3} s^{-1}	[104]
k_{13}	Dimerization of P	10^{-5} m^{-1} s^{-1}	[104]
k_{-13}	Dissociation of P	10^{-5} s^{-1}	[104]
k_D	Autoinducer diffusivity	0.23 s^{-1}	[110] and [111]
k_{tr}	GFP protein production	4.16×10^{-2} s^{-1}	[112]
k_{Gm}	GFP maturation	10^{-3} s^{-1}	[112]
k_{Gd}	GFP degradation	1.15×10^{-3} s^{-1}	[112]

Although the illustrated layout captures the key intracellular dynamics and bistable switch-like behavior of the LuxIR network, real systems typically demonstrate higher complexity with supplementary positive and negative feedback loops. Thus, a more precise model can be achieved by the addition of these feedback loops to minimize the existing mismatch between the simulation and experimental results. More specifically, the transcription factor also activates expression of the LuxR protein resulting in an additional positive feedback loop which was not modeled in the minimal network model. The other possible reasons for any mismatch between

the experimental and computational data may originate from the type of medium that is used for the QS assays and/or the different availability of oxygen for the bacteria samples in closed channels compared to open microtiter plates. Also, it should be noted that an additional component considering the degradation of the autoinducer molecules can be added to eqn. (B-5) if it is relevant to the timeline of the simulation given the chemical composition and pH of the medium.

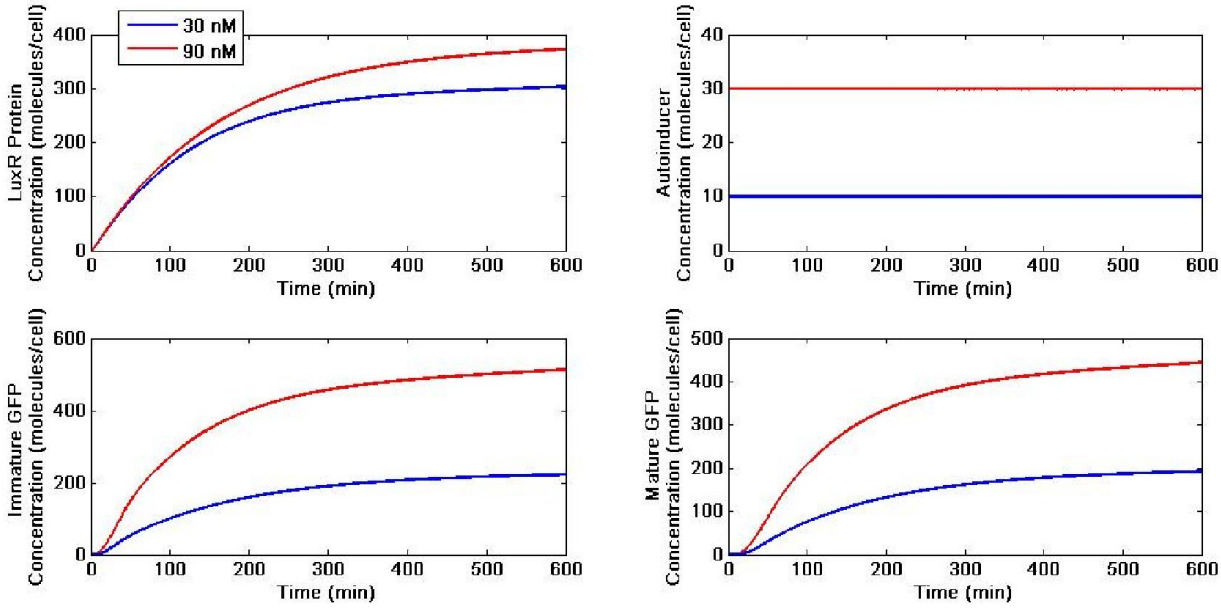

Figure B.5: Modeled response in the LuxIR quorum-sensing network at 30 nM and 90 nM extracellular concentrations of AHL. The time-evolution of the (a) LuxR regulatory protein, (b) intracellular concentration of the autoinducer, (c) immature GFP, and (d) mature GFP.

Chapter 5: Microfluidic-based characterization of quorum-sensing response in a chemotactic sender-receiver network

Abstract

Exploiting synthetic QS-based circuits, coordinated group activities such as delivery of small molecules or cancer invasion can be launched from a localized population of engineered BacteriaBots in response to environmental cues. Characterization of QS-regulated behaviors of swimming bacteria is critical to understanding of collaborative task performance by BacteriaBots. Here, the hydrogel-based microfluidic device previously used for the chemotaxis studies enabled us to characterize the QS behavior of a chemotactic population of receiver-only *Escherichia coli* MG1655 bacteria in response to the signaling molecules released from the localized AHL-sending *E. coli* MG1655. The QS genes in the receiver *E. coli* MG1655 bacteria are functionally linked with a fluorescent reporter to ease the quantification of the response. Such experimental characterization of bacterial QS response can foster applications in bionanomedicine and biosensing and advance our understanding of the effective calling distance over which sender and receiver BacteriaBots can communicate with each other to perform pre-programmed tasks towards fulfilling the development of an autonomous network of bacteria-based bio-hybrid cargo delivery vehicles.

5.1 Introduction

Synthetic biology has provided the tools for modulating existing biological networks and/or constructing recombinant plasmids to enable the host cells to perform novel tasks such as QS in addition to their innate cellular processes [53, 54]. For example, the transfer of the whole or a part of the LuxI/LuxR genetic system from *Vibrio fischeri* to *E. coli* has programmed the transformant to acquire QS-induced programmed population control via regulated killing of cells [58], and invasion of cancer cells [60]. Others have demonstrated also the construction of QS-based synthetic sender-receiver systems including artificial multicellular system capable of programmed pattern formation, motility switch and biofilm modeling [56, 59, 113]. Here, it is demonstrated that the previously fabricated hydrogel-based microfluidic device can be used for characterizing the QS response of a chemotactic population of AHL-receiving bacteria in response to AHL-sending bacteria. For this purpose, the quorum-sensing response in receiver-only (*luxI*⁻) *E. coli* MG1655R in the presence of the homoserine lactone molecules produced by *E. coli* MG1655 transformed with the LuxI autoinducer synthase was characterized. This characterization is critical to development of a myriad of bacteria-enabled systems including BacteriaBots that are envisioned to execute cooperative theranostic tasks at targeted disease sites by harnessing BacteriaBot-BacteriaBot communication.

5.2 Materials and methods

5.2.1 Microfluidic assay

A different size of our recently reported diffusion-based poly(ethylene glycol) diacrylate (PEG-DA) microfluidic device described in Section 3.2.2 (700 μm wide channels and hydrogel walls) was fabricated to create temporally invariant concentration gradients of casamino acids, a known

chemoattractant mixture for *E. coli* K-12. The microfluidic device was sterilized under UV light for 20 min prior to the experiment. The device was then washed with sterile 1× phosphate buffered saline solution. The medium that was used for the chemotaxis/QS experiments was a 1:9 ratio of the RM medium (1 × M9 salts, 2% casamino acids, and 0.4% glucose) [101] and a modified motility buffer with an elevated concentration of glucose (0.4%) (see 3.2.1 for motility buffer recipe), hereafter called modified RM medium, to satisfy the requirements for both BacteriaBot construction and induction of QS response and also have the same glucose concentration in every single position in the channels and the hydrogel walls. The modified RM medium was injected in the center channel and the corresponding tube was clamped afterwards to prevent any fluid flow and liquid evaporation. The linear gradients of casamino acids were established by continuously flowing the chemoattractant solution (0.7% (w/v) in modified RM medium) and the blank modified RM medium in the two feeder channels at 5 μl min^{-1}, and by lateral diffusion of the chemoattractant through the hydrogel walls and into the flow-free buffer-filled center channel. The linear chemical gradient was maintained in the middle channel for the entire duration of experiment.

5.2.2 Bacteria and plasmids

Motile isolates of *E. coli* MG1655 (i.e. MG1655m) were transformed with the AHL-responsive segment of the LuxIR network from *V. fischeri* through inserting the pLVA01 plasmid construct (Ap^r; pUC18Not-*luxR*-P_{luxI}-RBSII-*gfp*(LVA)-T_0-T_1) [91] into the bacteria using standard protocols [81]. A similar protocol was used to insert the sender plasmid, pBLH305 [114], into the same bacterial strain to make the sender cells, hereafter called MG1655S. The *E. coli* MG1655R and MG1655S bacteria, generated as described above, were grown overnight at 30 ˚C

and 150 rpm shaking in 10 ml of LB broth supplemented with ampicillin for MG1655R (100 μg ml^{-1}) and chloramphenicol for MG1655S (20 μg ml^{-1}) and then diluted 1:100 in LB medium to start fresh bacterial cultures. When the bacterial cultures reached an OD_{600} of 1.0, 1 ml of each bacterial culture was harvested by centrifugation at 1,700 × g for 5 min and the resultant pellets were resuspended in 1 ml of the modified RM medium. The sender cells suspension was washed two times to remove the free autoinducers. Lastly, 100 μl of the receiver bacteria suspension was mixed with 100 μl of the sender cells and 800 μl of blank modified RM medium (to dilute both bacteria at 10:1) and loaded in a 1 ml syringe, injected into the center channel of the device replacing the blank modified RM medium. Moreover, the effect of doubling the number of senders on the QS response in the receivers was studied by making the 1 ml samples using 200 μl of the sender cells suspension.

5.2.3 Data analysis

All of the experiments were conducted at 30 ˚C using a Zeiss Axio-observer Z1 inverted fluorescence microscope equipped with a climate control incubation chamber. Fluorescence images of the swimming bacteria were acquired every 30 min for a total of 6 hours using a 10× objective lens. Experiments were conducted in triplicates and microscopy images were acquired from three independent sections of the middle channel. The exposure time of fluorescent images was 200 ms. In order to quantify the QS response of bacteria, the width of the center channel was divided in two halves and the total fluorescence response in the half near the chemoattractant side was measured using the ImageJ software.

5.3 Results and discussion

Circuit operation of the sender-receiver system used in this work is illustrated in Fig. 5.1. In this system, AHL is produced by LuxI autoinducer synthase of the *E. coli* MG1655S bacteria and released in the extracellular environment. At a critical concentration of accumulated AHL, the autoinducer molecule (i.e. 3-oxo-C6-HSL) binds specifically to the LuxR regulatory protein in the *E. coli* MG1655R bacteria and this complex regulates downstream genes upon binding to the *lux* box region activating GFP expression. Utilizing the microfluidic device fabricated in the previous section, the QS behavior in the chemotactic population of the receivers for equal and doubled number of the sender cells was characterized here. The three-channel microfluidic platform mimics the natural systems where diffusion is the only determining factor affecting local autoinducer concentrations and buildup of the autoinducers due to the lack of flow triggers the QS response in bacteria. The time-response curves associated with the evolution of QS in the receiver bacteria are plotted in Fig. 5.2 (a). As illustrated, when the number of sender bacteria increases, the AHL concentration also increases in the microenvironment that localized chemotactic bacteria are present. This elevated autoinducer concentration induces a stronger QS fluorescence response in the receiver bacteria. The difference between the QS response of the receiver bacteria in the presence of equal and doubled number of the sender cells becomes statistically significant after 90 min of conducting the experiment ($p<0.01$, one-way ANOVA and Tukey's test). In all of the experiments, there is no immediate impermeable boundary for the AHL molecules and they can easily diffuse away from the bacteria into the hydrogel walls. Representative images of the QS-directed fluorescent response of the chemotactic swimming bacteria in the center channel of the microfluidic device are shown in Fig. 5.2 (b). This characterization of the QS response of a localized population of swimming *E. coli* MG1655R

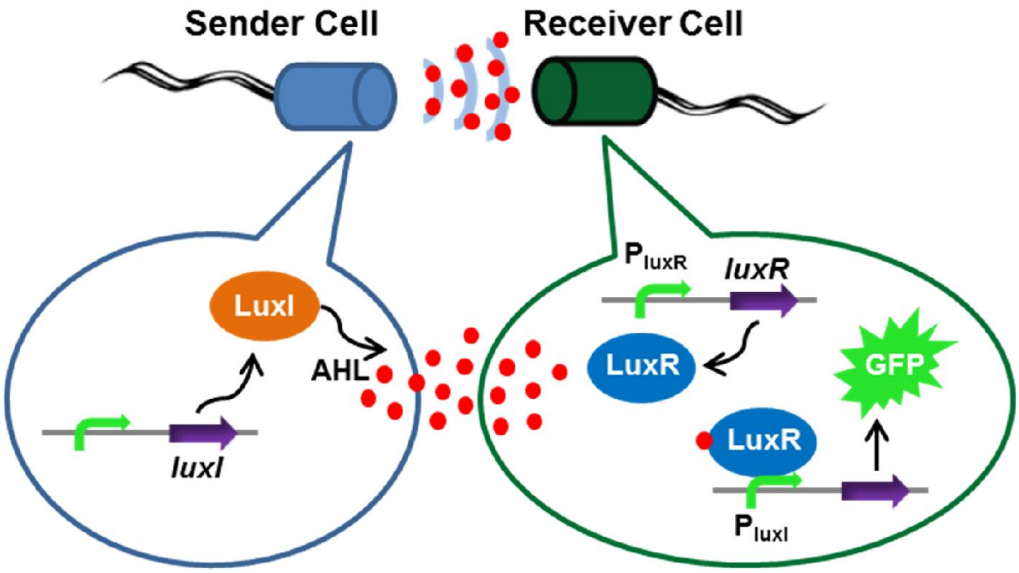

Figure 5.1 Circuit operation of the LuxI/LuxR sender-receiver system.

bacteria enables us to predict the coordinated behavior of a mobile network of receiver-only BacteriaBots as part of a sender-receiver system in which sender BacteriaBots transmit the signals and receiver BacteriaBots perform the pre-programmed multi-agent task(s) at the target site.

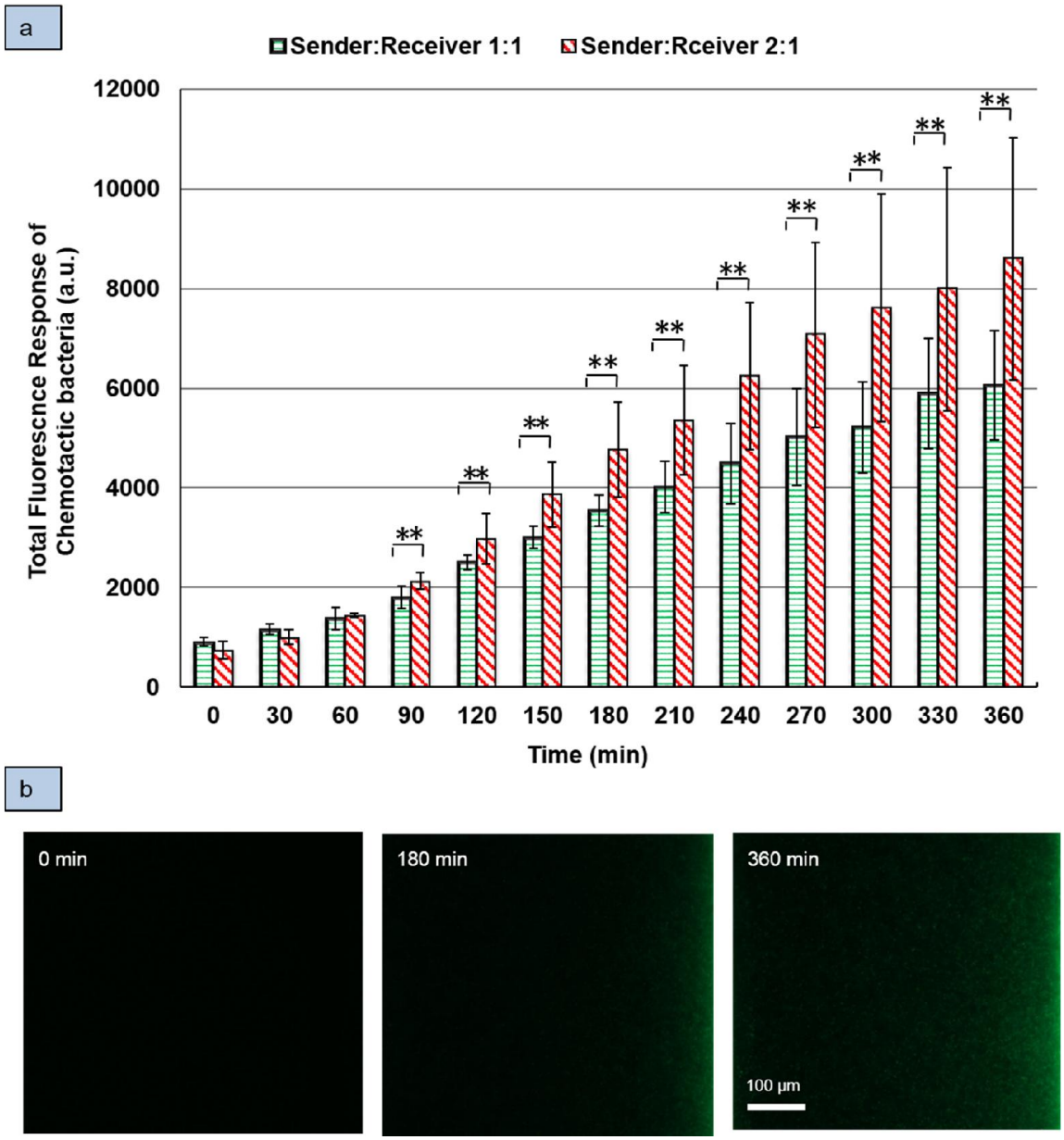

Figure 5.2 (a) Total fluorescence response of *E. coli* MG1655R in the right half of the center channel near the chemoattractant side. The error bars represent standard deviation (n=6); (b) Representative fluorescent images illustrating the time-evolution of the QS response of receiver bacteria in a chemotactic mixed population of receiver and sender bacteria.

5.4 Conclusions

In this study, the QS response of a bioreporter, (*luxI*$^-$) *E. coli* MG1655R containing the GFP-expressing pLVA01 plasmid, was characterized using a diffusion-based microfluidic platform. The QS signals were naturally produced by (*luxI*$^+$) sender *E. coli* MG1655S bacteria containing the pBLH305 plasmid. This characterization lays the foundation for predicting the collaborative behavior of a mobile network of BacteriaBots when the sender and receiver bacteria are pre-programmed with QS-based genetic circuits. The well-characterized BacteriaBots can participate in coordinated group activities to accomplish autonomously directed tasks at the target site. The proposed platform will also help discover the physical, chemical and biological parameters governing QS systems in the light organs of marine animals as well as biofilms present in infectious diseases where large populations of bacteria exist and diffusion is the dominant means of autoinducer transport.

Chapter 6: Conclusions and future directions

The main goal of this dissertation work was to develop and characterize a mobile network of bacteria-based bio-hybrid cargo delivery systems. This was achieved through the completion of the main following research tasks: (1) Construction of a new library of bacteria-assisted cargo delivery systems by coupling live engineered bacteria with the fabricated non-spherical particles. (2) Characterization of the BacteriaBots transport in an isotropic environment as well as in the presence of chemical cues. (3) Characterization of bacterial cell-cell communication network in order to understand the coordinated behavior of a population of BacteriaBots. The work presented in this dissertation lays the foundation for development of a well-characterized generation of bacteria-assisted cargo delivery devices with enhanced transport properties and capable of executing pre-programmed multi-agent coordinated tasks upon their arrival at the target site.

6.1 Concluding Remarks

Dissertation findings and original contributions

A collection of cargo carrying agents comprised of on-spherical microparticles interfaced with live engineered bacteria, named as BacteriaBots, was constructed here by utilizing a currently existing high-throughput particle casting and stretching technique. First, prolate spheroid, barrel, and bullet-shaped polystyrene microparticles were fabricated and conjugated with motile isolates of *E. coli* MG1655 bacteria using poly-L-lysine. Next, the influence of body shape on the dynamics of the motile BacteriaBots was investigated for the first time. Non-spherical geometries was shown to increase the mean directionality of the motion of the BacteriaBots but

does not significantly affect their average speed compared with their spherical counterparts. Moreover, directionality of non-spherical BacteriaBots was shown to be dependent on the aspect ratio of the body and for the case of prolate spheroid, a higher aspect ratio of two led to a larger directionality compared to their low aspect ratio counterparts. The additional theoretical analysis supported the experimental results showing that self-propelled prolate spheroids experience two directionally different translational coefficients of drag which results in a more directional motion path compared to the spherical counterparts. In the next step, a group of BacteriaBots with spherical/non-spherical geometries was developed taking advantage of the strong non-covalent streptavidin-biotin bond. The anti-*E. coli* antibody used here resulted in the attachment of the antibody-decorated bacteria to the streptavidin-coated particles only through their cell bodies (and not their flagella). The chemotactic behavior of spherical and elliptical disk-shaped BacteriaBots was then characterized in the presence of linear gradients of L-aspartic acid inside a diffusion-based microfluidic chemotaxis assay device. The experimental results demonstrate for the first time that bacterial chemotactic response dominates the effect of body shape in the absence of fluid flow; thus, it can be concluded that the non-spherical system could be more favorable for drug delivery applications owing to the known benefits of using non-spherical particles for vascular transport (e.g. relatively long circulation time). Moreover, it was shown that the dominance of chemical steering over body shape was not disrupted by changing the chemical concentration gradient slope.

In addition to engineering the body shape of the BacteriaBots, the biotic component of the system (i.e. bacteria) was also engineered with synthetic quorum-sensing based genetic circuits to enable execution of cooperative theranostic tasks at targeted disease sites by harnessing bacterial cell-cell communication. For this purpose, the motility-enhanced *E. coli* MG1655 was

transformed with the AHL-responsive segment of the LuxIR network (from *V. fischeri*) linked to a GFP reporter. The quorum-sensing response of this genetically modified bacterial strain in the presence a wide range of concentrations of the exogenous signaling molecules was then characterized in a high-throughput microfluidic platform. Such experimental characterization of bacterial QS helps us predict the effective calling distance over which BacteriaBots can communicate with each other and design more advanced novel functionalities for a variety of end applications. Moreover, a relevant mathematical model of the AHL-responsive segment of the LuxIR network was developed in the form of a system of ordinary differential equations (ODEs). The simulation results support the trend of the response observed in the microfluidic experiments. Lastly, the quorum-sensing behavior of a sender-receiver network of bacteria was characterized in a microenvironment that mimics near *in-vivo* conditions where the agents localize at the targeted site and begin to carry out pre-programmed functions. The preliminary results for this characterization was one more step towards fulfilling the development of an autonomous network of bacteria-based bio-hybrid delivery vehicles. Use of non-spherical particles combined with the invasive and signaling properties of motile bacteria provides a new spectrum of solutions for designing autonomous carriers with higher efficiency for rapidly evolving nanomedicine applications.

6.2 Future directions

The work presented in this dissertation can be expanded to help solve bioengineering and biological problems of significance. A few possible directions are outlined as below:

1. **Validation and/or prediction of the QS-based phenotypic behaviors of bacteria/BacteriaBots via computational simulation**

   Development of a computational simulator of the QS response of chemotactic bacteria/BacteriaBots in the presence of QS signaling molecules not only helps validate the experimental results of the receiver-only and sender-receiver systems, but also allows predicting the output of similar or related systems. For this purpose, chemical kinetics of intracellular signaling of bacteria needs to be coupled with suitable models of autoinducer diffusion and bacteria/BacteriaBots motility to create a comprehensive computational model that can closely mimic the experimental conditions in which BacteriaBots are distributed in a biased fashion due to chemotaxis as they are connected via chemical signals.

2. **Investigating the penetration and distribution of BacteriaBots with tailored shape in multicellular tumor spheroids**

   BacteriaBots with non-spherical geometries will be fabricated using different sizes of polystyrene particles and different bacterial species; *E. coli* MG1655m and *S.* Typhimurium VNP20009. Three-dimensional *in-vitro* multicellular tumor spheroids (MCTs) can be used to investigate intratumoral transport and distribution of spherical and non-spherical BacteriaBots. Finding from such *in-vitro* studies, will provide invaluable insight into design and fabrication of BacteriaBots with optimal body geometry for cancer treatment/diagnostic applications.

3. **Developing BacteriaBots with a variety of advanced functionalities through transformation with QS-based genetic circuits**

Toxin-antitoxin (TA) modules are present in almost all free-living bacterial species that have been sequenced including *E. coli* bacteria. A TA module typically consists of genes encoding a toxin and an antitoxin that neutralizes the toxin [115]. Under stressful conditions such as amino acid starvation [116], antibiotic treatment [117] or oxidative stress [118], antitoxins are quickly degraded, thus freeing toxins to apply their poisoning effects. The resulting programmed cell death of the bacterial population will be regulated through simultaneous synthesis of death and survival proteins. This innate module which can be activated under stressful conditions or synthetic QS-based regulated killing circuits which can be transferred into bacteria [58], can help control the bacterial population number and prevent undesirable outcomes including septic shock of the host when BacteriaBots target cancerous regions. Using such engineered bacteria, BacteriaBots will be able to perform a variety of advanced pre-programmed coordinated tasks of interest after reaching the target site.

Bibliography

[1] Behkam B, Sitti M. Bacteria integrated swimming microrobots. 50 years of artificial intelligence: Springer; 2007. p. 154-63.

[2] Zhang L, Abbott JJ, Dong L, Kratochvil BE, Bell D, Nelson BJ. Artificial bacterial flagella: Fabrication and magnetic control. Applied Physics Letters 2009;94:064107--3.

[3] Dreyfus R, Baudry J, Roper ML, Fermigier M, Stone HA, Bibette J. Microscopic artificial swimmers. Nature 2005;437:862-5.

[4] Steager E, Kim C-B, Patel J, Bith S, Naik C, Reber L, et al. Control of microfabricated structures powered by flagellated bacteria using phototaxis. Applied Physics Letters 2007;90:263901--3.

[5] Behkam B, Sitti M. Bacterial flagella-based propulsion and on/off motion control of microscale objects. Applied Physics Letters 2007;90:023902--3.

[6] Weibel DB, Garstecki P, Ryan D, DiLuzio WR, Mayer M, Seto JE, et al. Microoxen: Microorganisms to move microscale loads. Proceedings of the National Academy of Sciences USA 2005;102:11963-7.

[7] Darnton N, Turner L, Breuer K, Berg HC. Moving fluid with bacterial carpets. Biophysical Journal 2004;86:1863-70.

[8] Martel S, Tremblay CC, Ngakeng S, Langlois G. Controlled manipulation and actuation of micro-objects with magnetotactic bacteria. Applied Physics Letters 2006;89:233904--3.

[9] Fernandes R, Zuniga M, Sassine FR, Karakoy M, Gracias DH. Enabling cargo-carrying bacteria via surface attachment and triggered release. Small 2011;7:588-92.

[10] Tanaka Y, Morishima K, Shimizu T, Kikuchi A, Yamato M, Okano T, et al. An actuated pump on-chip powered by cultured cardiomyocytes. Lab on a Chip 2006;6:362-8.

[11] Tao L, Hu W, Liu Y, Huang G, Sumer BD, Gao J. Shape-specific polymeric nanomedicine: emerging opportunities and challenges. Experimental Biology and Medicine 2011;236:20-9.

[12] Muro S, Garnacho C, Champion JA, Leferovich J, Gajewski C, Schuchman EH, et al. Control of endothelial targeting and intracellular delivery of therapeutic enzymes by modulating the size and shape of ICAM-1-targeted carriers. Molecular Therapy 2008;16:1450-8.

[13] Park JH, von Maltzahn G, Zhang L, Derfus AM, Simberg D, Harris TJ, et al. Systematic surface engineering of magnetic nanoworms for in vivo tumor targeting. Small 2009;5:694-700.

[14] Park JH, von Maltzahn G, Zhang L, Schwartz MP, Ruoslahti E, Bhatia SN, et al. Magnetic iron oxide nanoworms for tumor targeting and imaging. Advanced Materials 2008;20:1630-5.

[15] Geng Y, Dalhaimer P, Cai S, Tsai R, Tewari M, Minko T, et al. Shape effects of filaments versus spherical particles in flow and drug delivery. Nature Nanotechnology 2007;2:249-55.

[16] Gratton SE, Ropp PA, Pohlhaus PD, Luft JC, Madden VJ, Napier ME, et al. The effect of particle design on cellular internalization pathways. Proceedings of the National Academy of Sciences USA 2008;105:11613-8.

[17] Champion JA, Katare YK, Mitragotri S. Making polymeric micro-and nanoparticles of complex shapes. Proceedings of the National Academy of Sciences USA 2007;104:11901-4.

[18] Ho C, Keller A, Odell J, Ottewill R. Preparation of monodisperse ellipsoidal polystyrene particles. Colloid and Polymer Science 1993;271:469-79.

[19] Thakor AS, Gambhir SS. Nanooncology: The future of cancer diagnosis and therapy. CA: A Cancer Journal for Clinicians 2013;63:395-418.

[20] Ferrari M. Cancer nanotechnology: opportunities and challenges. Nature Reviews Cancer 2005;5:161-71.

[21] Adriani G, de Tullio MD, Ferrari M, Hussain F, Pascazio G, Liu X, et al. The preferential targeting of the diseased microvasculature by disk-like particles. Biomaterials 2012;33:5504-13.

[22] Decuzzi P, Pasqualini R, Arap W, Ferrari M. Intravascular delivery of particulate systems: does geometry really matter? Pharmaceutical Research 2009;26:235-43.

[23] Canelas DA, Herlihy KP, DeSimone JM. Top-down particle fabrication: control of size and shape for diagnostic imaging and drug delivery. Wiley Interdisciplinary Reviews: Nanomedicine and Nanobiotechnology 2009;1:391-404.

[24] Peer D, Karp JM, Hong S, Farokhzad OC, Margalit R, Langer R. Nanocarriers as an emerging platform for cancer therapy. Nature Nanotechnology 2007;2:751-60.

[25] Maeda H, Wu J, Sawa T, Matsumura Y, Hori K. Tumor vascular permeability and the EPR effect in macromolecular therapeutics: a review. Journal of Controlled Release 2000;65:271-84.

[26] Timko BP, Dvir T, Kohane DS. Remotely triggerable drug delivery systems. Advanced Materials 2010;22:4925-43.

[27] Fleige E, Quadir MA, Haag R. Stimuli-responsive polymeric nanocarriers for the controlled transport of active compounds: concepts and applications. Advanced Drug Delivery Reviews 2012;64:866-84.

[28] Kasinskas RW, Forbes NS. *Salmonella* Typhimurium lacking ribose chemoreceptors localize in tumor quiescence and induce apoptosis. Cancer Research 2007;67:3201-9.

[29] Leschner S, Weiss S. *Salmonella*—allies in the fight against cancer. Journal of Molecular Medicine 2010;88:763-73.

[30] Pawelek JM, Low KB, Bermudes D. Bacteria as tumour-targeting vectors. The Lancet Oncology 2003;4:548-56.

[31] Akin D, Sturgis J, Ragheb K, Sherman D, Burkholder K, Robinson JP, et al. Bacteria-mediated delivery of nanoparticles and cargo into cells. Nature Nanotechnology 2007;2:441-9.

[32] Vassaux G, Nitcheu J, Jezzard S, Lemoine NR. Bacterial gene therapy strategies. The Journal of Pathology 2006;208:290-8.

[33] Stritzker J, Weibel S, Seubert C, Götz A, Tresch A, Van Rooijen N, et al. Enterobacterial tumor colonization in mice depends on bacterial metabolism and macrophages but is independent of chemotaxis and motility. International Journal of Medical Microbiology 2010;300:449-56.

[34] Weibel S, Stritzker J, Eck M, Goebel W, Szalay AA. Colonization of experimental murine breast tumours by *Escherichia coli* K-12 significantly alters the tumour microenvironment. Cellular Microbiology 2008;10:1235-48.

[35] Heimann DM, Rosenberg SA. Continuous intravenous administration of live genetically modified *Salmonella* Typhimurium in patients with metastatic melanoma. Journal of Immunotherapy (Hagerstown, Md: 1997) 2003;26:179.

[36] Toso JF, Gill VJ, Hwu P, Marincola FM, Restifo NP, Schwartzentruber DJ, et al. Phase I study of the intravenous administration of attenuated *Salmonella* Typhimurium to patients with metastatic melanoma. Journal of Clinical Oncology 2002;20:142-52.

[37] Yoo J-W, Irvine DJ, Discher DE, Mitragotri S. Bio-inspired, bioengineered and biomimetic drug delivery carriers. Nature Reviews Drug Discovery 2011;10:521-35.

[38] Behkam B. Bacteria as actuators for hybrid (biotic/abiotic) swimming micro-robots: Design, modeling, and implementation: ProQuest; 2008.

[39] Fuqua WC, Winans SC, Greenberg EP. Quorum sensing in bacteria: the LuxR-LuxI family of cell density-responsive transcriptional regulators. Journal of Bacteriology 1994;176:269.

[40] Miller MB, Bassler BL. Quorum sensing in bacteria. Annual Reviews in Microbiology 2001;55:165-99.

[41] Pacheco AR, Sperandio V. Inter-kingdom signaling: chemical language between bacteria and host. Current Opinion in Microbiology 2009;12:192-8.

[42] Fuqua C, Greenberg EP. Listening in on bacteria: acyl-homoserine lactone signalling. Nature Reviews Molecular Cell Biology 2002;3:685-95.

[43] Decho AW, Frey RL, Ferry JL. Chemical challenges to bacterial AHL signaling in the environment. Chemical Reviews 2010;111:86-99.

[44] Donlan RM, Costerton JW. Biofilms: survival mechanisms of clinically relevant microorganisms. Clinical Microbiology Reviews 2002;15:167-93.

[45] Daniels R, Vanderleyden J, Michiels J. Quorum sensing and swarming migration in bacteria. FEMS Microbiology Reviews 2004;28:261-89.

[46] Parsek MR, Greenberg E. Sociomicrobiology: the connections between quorum sensing and biofilms. Trends in Microbiology 2005;13:27-33.

[47] Nealson KH, Platt T, Hastings JW. Cellular control of the synthesis and activity of the bacterial luminescent system. Journal of Bacteriology 1970;104:313-22.

[48] Winzer K, Williams P. Quorum sensing and the regulation of virulence gene expression in pathogenic bacteria. International Journal of Medical Microbiology 2001;291:131-43.

[49] Ng W-L, Bassler BL. Bacterial quorum-sensing network architectures. Annual Review of Genetics 2009;43:197-222.

[50] Eberhard A, Burlingame A, Eberhard C, Kenyon G, Nealson K, Oppenheimer N. Structural identification of autoinducer of *Photobacterium fischeri* luciferase. Biochemistry 1981;20:2444-9.

[51] Egland KA, Greenberg E. Quorum sensing in *Vibrio fischeri*: elements of the *luxI* promoter. Molecular Microbiology 1999;31:1197-204.

[52] Nealson KH. Autoinduction of bacterial luciferase. Archives of Microbiology 1977;112:73-9.

[53] Voigt CA. Genetic parts to program bacteria. Current Opinion in Biotechnology 2006;17:548-57.

[54] Pai A, Tanouchi Y, Collins CH, You L. Engineering multicellular systems by cell–cell communication. Current Opinion in Biotechnology 2009;20:461-70.

[55] Hooshangi S, Bentley WE. From unicellular properties to multicellular behavior: bacteria quorum sensing circuitry and applications. Current Opinion in Biotechnology 2008;19:550-5.

[56] Weiss LE, Badalamenti JP, Weaver LJ, Tascone AR, Weiss PS, Richard TL, et al. Engineering motility as a phenotypic response to LuxI/R-dependent quorum sensing in *Escherichia coli*. Biotechnology and Bioengineering 2008;100:1251-5.

[57] Kobayashi H, Kærn M, Araki M, Chung K, Gardner TS, Cantor CR, et al. Programmable cells: interfacing natural and engineered gene networks. Proceedings of the National Academy of Sciences USA 2004;101:8414-9.

[58] You L, Cox RS, Weiss R, Arnold FH. Programmed population control by cell–cell communication and regulated killing. Nature 2004;428:868-71.

[59] Basu S, Gerchman Y, Collins CH, Arnold FH, Weiss R. A synthetic multicellular system for programmed pattern formation. Nature 2005;434:1130-4.

[60] Anderson JC, Clarke EJ, Arkin AP, Voigt CA. Environmentally controlled invasion of cancer cells by engineered bacteria. Journal of Molecular Biology 2006;355:619-27.

[61] Berg HC, Brown DA. Chemotaxis in *Escherichia coli* analysed by three-dimensional tracking. Nature 1972;239:500-4.

[62] Berg HC. Random walks in biology: Princeton University Press; 1993.

[63] Traoré MA, Sahari A, Behkam B. Computational and experimental study of chemotaxis of an ensemble of bacteria attached to a microbead. Physical Review E 2011;84:061908.

[64] Paglia P, Medina E, Arioli I, Guzman CA, Colombo MP. Gene transfer in dendritic cells, induced by oral DNA vaccination with *Salmonella* Typhimurium, results in protective immunity against a murine fibrosarcoma. Blood 1998;92:3172-6.

[65] Darji A, Guzmán CA, Gerstel B, Wachholz P, Timmis KN, Wehland J, et al. Oral somatic transgene vaccination using attenuated *S.* Typhimurium. Cell 1997;91:765-75.

[66] Sizemore DR, Branstrom AA, Sadoff JC. Attenuated Shigella as a DNA delivery vehicle for DNA-mediated immunization. Science 1995;270:299-303.

[67] Yong AY, Shabahang S, Timiryasova TM, Zhang Q, Beltz R, Gentschev I, et al. Visualization of tumors and metastases in live animals with bacteria and vaccinia virus encoding light-emitting proteins. Nature Biotechnology 2004;22:313-20.

[68] Nuyts S, Van Mellaert L, Theys J, Landuyt W, Lambin P, Anné J. Clostridium spores for tumor-specific drug delivery. Anti-Cancer Drugs 2002;13:115-25.

[69] Barker CS, Prüß BM, Matsumura P. Increased motility of *Escherichia coli* by insertion sequence element integration into the regulatory region of the *flhD* operon. Journal of Bacteriology 2004;186:7529-37.

[70] ten Hagen B, van Teeffelen S, Löwen H. Brownian motion of a self-propelled particle. Journal of Physics: Condensed Matter 2011;23:194119.

[71] Han Y, Alsayed A, Nobili M, Yodh AG. Quasi-two-dimensional diffusion of single ellipsoids: Aspect ratio and confinement effects. Physical Review E 2009;80:011403.

[72] Happel J, Brenner H. Low Reynolds number hydrodynamics: with special applications to particulate media. Springer; 1983.

[73] Behkam B, Sitti M. Effect of quantity and configuration of attached bacteria on bacterial propulsion of microbeads. Applied Physics Letters 2008;93:223901.

[74] Loessner H, Endmann A, Leschner S, Westphal K, Rohde M, Miloud T, et al. Remote control of tumour-targeted *Salmonella enterica* serovar Typhimurium by the use of l-arabinose as inducer of bacterial gene expression in vivo. Cellular Microbiology 2007;9:1529-37.

[75] Stritzker J, Weibel S, Hill PJ, Oelschlaeger TA, Goebel W, Szalay AA. Tumor-specific colonization, tissue distribution, and gene induction by probiotic Escherichia coli Nissle 1917 in live mice. International Journal of Medical Microbiology 2007;297:151-62.

[76] Sahari A, Headen D, Behkam B. Effect of body shape on the motile behavior of bacteria-powered swimming microrobots (BacteriaBots). Biomedical Microdevices 2012;14:999-1007.

[77] Park SJ, Bae H, Kim J, Lim B, Park J, Park S. Motility enhancement of bacteria actuated microstructures using selective bacteria adhesion. Lab on a Chip 2010;10:1706-11.

[78] Berg HC, Turner L. Torque generated by the flagellar motor of Escherichia coli. Biophysical journal 1993;65:2201-16.

[79] Traore MA, Behkam B. A PEG-DA microfluidic device for chemotaxis studies. Journal of Micromechanics and Microengineering 2013;23:085014.

[80] Cheng H-P, Walker GC. Succinoglycan is required for initiation and elongation of infection threads during nodulation of alfalfa by *Rhizobium meliloti*. Journal of Bacteriology 1998;180:5183-91.

[81] Sambrook J, Fritsch EF, Maniatis T. Molecular cloning: Cold Spring Harbor Laboratory Press New York; 1989.

[82] Mao H, Cremer PS, Manson MD. A sensitive, versatile microfluidic assay for bacterial chemotaxis. Proceedings of the National Academy of Sciences USA 2003;100:5449-54.

[83] Segall JE, Block SM, Berg HC. Temporal comparisons in bacterial chemotaxis. Proceedings of the National Academy of Sciences USA 1986;83:8987-91.

[84] Springer MS, Goy MF, Adler J. Sensory transduction in Escherichia coli: two complementary pathways of information processing that involve methylated proteins. Proceedings of the National Academy of Sciences USA 1977;74:3312-6.

[85] Weber PC, Ohlendorf D, Wendoloski J, Salemme F. Structural origins of high-affinity biotin binding to streptavidin. Science 1989;243:85-8.

[86] Redfield RJ. Is quorum sensing a side effect of diffusion sensing? Trends in Microbiology 2002;10:365-70.

[87] Yan L, Allen MS, Simpson ML, Sayler GS, Cox CD. Direct quantification of N-(3-oxo-hexanoyl)-l-homoserine lactone in culture supernatant using a whole-cell bioreporter. Journal of Microbiological Methods 2007;68:40-5.

[88] Brelles-Mariño G, Bedmar EJ. Detection, purification and characterisation of quorum-sensing signal molecules in plant-associated bacteria. Journal of Biotechnology 2001;91:197-209.

[89] Hense BA, Kuttler C, Müller J, Rothballer M, Hartmann A, Kreft J-U. Does efficiency sensing unify diffusion and quorum sensing? Nature Reviews Microbiology 2007;5:230-9.

[90] Flickinger ST, Copeland MF, Downes EM, Braasch AT, Tuson HH, Eun Y-J, et al. Quorum sensing between *Pseudomonas aeruginosa* biofilms accelerates cell growth. Journal of the American Chemical Society 2011;133:5966-75.

[91] Groisman A, Lobo C, Cho H, Campbell JK, Dufour YS, Stevens AM, et al. A microfluidic chemostat for experiments with bacterial and yeast cells. Nature Methods 2005;2:685-9.

[92] Carnes EC, Lopez DM, Donegan NP, Cheung A, Gresham H, Timmins GS, et al. Confinement-induced quorum sensing of individual Staphylococcus aureus bacteria. Nature Chemical Biology 2009;6:41-5.

[93] Boedicker JQ, Vincent ME, Ismagilov RF. Microfluidic confinement of single cells of bacteria in small volumes initiates high-density behavior of quorum sensing and growth and reveals its variability. Angewandte Chemie International Edition 2009;48:5908-11.

[94] Fernandes R, Roy V, Wu H-C, Bentley WE. Engineered biological nanofactories trigger quorum sensing response in targeted bacteria. Nature Nanotechnology 2010;5:213-7.

[95] Gantner S, Schmid M, Dürr C, Schuhegger R, Steidle A, Hutzler P, et al. In situ quantitation of the spatial scale of calling distances and population density-independent N-acylhomoserine lactone-mediated communication by rhizobacteria colonized on plant roots. FEMS Microbiology Ecology 2006;56:188-94.

[96] Geuther B, Behkam B. Towards quorum sensing based distributed control for networks of mobile sensors. Intelligent Robots and Systems (IROS), 2013 IEEE/RSJ International Conference on: IEEE; 2013. p. 1549-54.

[97] Kumari A, Pasini P, Deo SK, Flomenhoft D, Shashidhar H, Daunert S. Biosensing systems for the detection of bacterial quorum signaling molecules. Analytical Chemistry 2006;78:7603-9.

[98] Gauger EJ, Leatham MP, Mercado-Lubo R, Laux DC, Conway T, Cohen PS. Role of motility and the *flhDC* operon in *Escherichia coli* MG1655 colonization of the mouse intestine. Infection and Immunity 2007;75:3315-24.

[99] Jeon NL, Baskaran H, Dertinger SK, Whitesides GM, Van De Water L, Toner M. Neutrophil chemotaxis in linear and complex gradients of interleukin-8 formed in a microfabricated device. Nature Biotechnology 2002;20:826-30.

[100] Xia Y, Whitesides GM. Soft lithography. Annual Review of Materials Science 1998;28:153-84.

[101] Minogue TD, Trebra MWv, Bernhard F, Bodman SBv. The autoregulatory role of EsaR, a quorum-sensing regulator in *Pantoea stewartii ssp. stewartii*: evidence for a repressor function. Molecular Microbiology 2002;44:1625-35.

[102] Kim MJ, Breuer KS. Use of bacterial carpets to enhance mixing in microfluidic systems. Journal of Fluids Engineering 2007;129:319-24.

[103] Goryachev AB. Design principles of the bacterial quorum sensing gene networks. Wiley Interdisciplinary Reviews: Systems Biology and Medicine 2009;1:45-60.

[104] Goryachev A, Toh D, Lee T. Systems analysis of a quorum sensing network: design constraints imposed by the functional requirements, network topology and kinetic constants. Biosystems 2006;83:178-87.

[105] Dundr M, Hoffmann-Rohrer U, Hu Q, Grummt I, Rothblum LI, Phair RD, et al. A kinetic framework for a mammalian RNA polymerase in vivo. Science 2002;298:1623-6.

[106] Kierzek AM, Zaim J, Zielenkiewicz P. The effect of transcription and translation initiation frequencies on the stochastic fluctuations in prokaryotic gene expression. Journal of Biological Chemistry 2001;276:8165-72.

[107] Hambraeus G, von Wachenfeldt C, Hederstedt L. Genome-wide survey of mRNA half-lives in *Bacillus subtilis* identifies extremely stable mRNAs. Molecular Genetics and Genomics 2003;269:706-14.

[108] Iyer V, Struhl K. Absolute mRNA levels and transcriptional initiation rates in *Saccharomyces cerevisiae*. Proceedings of the National Academy of Sciences USA 1996;93:5208-12.

[109] Pratt JM, Petty J, Riba-Garcia I, Robertson DH, Gaskell SJ, Oliver SG, et al. Dynamics of protein turnover, a missing dimension in proteomics. Molecular & Cellular Proteomics 2002;1:579-91.

[110] Kaplan HB, Greenberg E. Diffusion of autoinducer is involved in regulation of the *Vibrio fischeri* luminescence system. Journal of Bacteriology 1985;163:1210-4.

[111] Rubinow SI. Introduction to mathematical biology: Courier Dover Publications; 1975.

[112] Austin CM, Stoy W, Su P, Harber MC, Bardill JP, Hammer BK, et al. Modeling and validation of autoinducer-mediated bacterial gene expression in microfluidic environments. Biomicrofluidics 2014;8:034116.

[113] Mirsaidov U, Scrimgeour J, Timp W, Beck K, Mir M, Matsudaira P, et al. Live cell lithography: using optical tweezers to create synthetic tissue. Lab on a Chip 2008;8:2174-81.

[114] Hanzelka BL, Stevens AM, Parsek MR, Crone TJ, Greenberg E. Mutational analysis of the *Vibrio fischeri* LuxI polypeptide: critical regions of an autoinducer synthase. Journal of Bacteriology 1997;179:4882-7.

[115] Pandey DP, Gerdes K. Toxin–antitoxin loci are highly abundant in free-living but lost from host-associated prokaryotes. Nucleic Acids Research 2005;33:966-76.

[116] Aizenman E, Engelberg-Kulka H, Glaser G. An *Escherichia coli* chromosomal "addiction module" regulated by guanosine [corrected] 3', 5'-bispyrophosphate: a model for programmed bacterial cell death. Proceedings of the National Academy of Sciences USA 1996;93:6059-63.

[117] Rice KC, Bayles KW. Death's toolbox: examining the molecular components of bacterial programmed cell death. Molecular Microbiology 2003;50:729-38.

[118] Hazan R, Sat B, Engelberg-Kulka H. *Escherichia coli* mazEF-mediated cell death is triggered by various stressful conditions. Journal of Bacteriology 2004;186:3663-9.